

VTT Technical Research Centre of Finland

Valorization of probabilistic seismic hazard results in Finland

Mäntyniemi, Päivi; Malm, Marianne; Rinne, Lauri; Fülöp, Ludovic

Published: 27/01/2023

Document Version
Publisher's final version

License
Other

[Link to publication](#)

Please cite the original version:

Mäntyniemi, P., Malm, M., Rinne, L., & Fülöp, L. (2023). *Valorization of probabilistic seismic hazard results in Finland*. VTT Technical Research Centre of Finland. VTT Research Report No. VTT-R-00978-22



VTT
<http://www.vtt.fi>
P.O. box 1000FI-02044 VTT
Finland

By using VTT's Research Information Portal you are bound by the following Terms & Conditions.

I have read and I understand the following statement:

This document is protected by copyright and other intellectual property rights, and duplication or sale of all or part of any of this document is not permitted, except duplication for research use or educational purposes in electronic or print form. You must obtain permission for any other use. Electronic or print copies may not be offered for sale.

RESEARCH REPORT

VTT-R-00978-22

Valorization of probabilistic seismic hazard results in Finland

Authors: Päivi Mäntyniemi¹, Marianne Malm², Lauri Rinne², Ludovic Fülöp³

¹Institute of Seismology, University of Helsinki

²AFRY Finland Oy

³VTT Technical Research Centre of Finland

Confidentiality: VTT Public

Version: 27.1.2023



beyond the obvious



Report's title Valorization of probabilistic seismic hazard results in Finland	
Customer, contact person, address The Finnish Nuclear Power Plant Safety Research Programme 2019–2022 (SAFIR2022)	Order reference VN/13467/2021
Project name Valorisation of the recent probabilistic seismic hazard projects and results (VN/13467/2021)	Project number/Short name VN/13467/2021 / VALERI
Author(s) Päivi Mäntyniemi, Marianne Malm, Lauri Rinne, Ludovic Fülöp	Pages 41
Keywords probabilistic seismic hazard analysis, nuclear regulations, design-basis earthquake, design extension condition, YVL guides	Report identification code VTT-R-00978-22
Summary <p>Probabilistic seismic hazard analysis (PSHA) is currently the standard method for assessing seismic hazards for nuclear power plants (NPPs) in Finland. To obtain values of ground-motion parameters for design purposes, two decisions are made regarding which annual frequency of exceedance (AFE) should be adopted and from which hazard curve the ground-motion value should be read for the design-basis earthquake (DBE) and the design-extension condition earthquake (DEC EQ, DEC C for short). The current regulatory status in Finland, given in the guide YVL B.7 (STUK 2019) by the Radiation and Nuclear Safety Authority of Finland (STUK), is that the median-confidence seismic hazard at AFE 10^{-5} is used for DBEs at NPPs with a minimum horizontal peak-ground acceleration (PGA) of 0.1 g. The high variability of ground-motion shaking patterns and various examples of exceedance of the DBE ground motion from that of natural earthquakes throughout the world have resulted in upgrades to meet new definitions of the requirements for ground motion beyond that of DBEs. Exceptional earthquake effects, with an estimated frequency of occurrence less than 10^{-5}/year are postulated in DEC C for NPPs in Finland.</p> <p>Here, we outline the PSHA and its consequent use in risk assessment and risk-informed decision-making. We review arguments about the mean and median hazard curves in the PSHA. We draw particularly on the outcomes of the SENSEI (SENsitivity study of SEismic hazard prediction in Finland) project conducted under the auspices of STUK in 2019–2020, present new figures based on the SENSEI set of hazard calculations, and analyze them. We focus on the ratio of the mean and median hazard of PGA, spectral acceleration at 1 Hz, 5 Hz, and 25 Hz at AFE levels 10^{-4}, 10^{-5}, 10^{-6}, 10^{-7} and 10^{-8}. We analyze possible options for DBE and DEC C for consideration of the various stakeholders. Since the use of median hazards has a long tradition in Finland, an update is no trivial undertaking. The suite of options is not necessarily exhaustive.</p>	
	VTT Public
Espoo, 27.1.2023 Written by on behalf of the authors Ludovic Fülöp Principal Scientist	Reviewed by Miguel Ferreira Research Team Leader
VTT's contact address VTT Technical Research Centre of Finland Ltd, P.O. Box 1000, FI-02044 VTT, Finland	
Distribution (customer and VTT) Customer VTT Archive	
<i>The use of the name of "VTT" in advertising or publishing of a part of this report is only permissible with written authorisation from VTT Technical Research Centre of Finland Ltd.</i>	



Approval

VTT TECHNICAL RESEARCH CENTRE OF FINLAND LTD

Date: 30.01.2023

Signature: The signature block contains a DocuSigned signature. It features the text 'DocuSigned by:' at the top, followed by the handwritten signature 'Marko Mäkipää' in black ink. Below the signature is the alphanumeric string 'EF95EB85E9804AC...'. The entire signature area is enclosed in a light beige rectangular box.

Name: Marko Mäkipää

Title: Research Team Leader



Preface

Here, we explore the association between probabilistic seismic hazard analysis (PSHA) and confidence-level results that are relevant to the design-basis earthquake (DBE) and the design-extension condition earthquake (DEC EQ, DEC C for short) for nuclear power plants (NPPs) in Finland. The high variability of ground-motion shaking patterns and various examples of exceedance of the DBE ground motion from natural earthquakes throughout the world have resulted in upgrades to meet new definitions of the requirements for ground motion beyond that of DBEs. The current regulatory status in Finland, given in the guide YVL B.7 (STUK 2019) by the Radiation and Nuclear Safety Authority of Finland (STUK), is that the median-confidence seismic hazard at an annual frequency of exceedance (AFE) 10^{-5} is used to substantiate the seismic DBE for NPPs, with a minimum horizontal peak ground acceleration value of 0.1 g. Exceptional external events and conditions with an estimated frequency of occurrence less than 10^{-5} /year are considered to be DEC C events. YVL B.7 states that hazard curves shall be presented at least up to the recurrence time of 10^7 years for the assessment of DEC C. The justificative memorandum of YVL B.7 (STUK 2019) further elaborates that an indicative value for DEC C could correspond to an AFE of $1 \cdot 10^{-7}$ /year, or an alternative limit for DEC C could be an acceleration approximately twice as large as the DBE acceleration.



Contents

Preface.....	3
1. Introduction.....	5
2. Calculation of seismic hazards using a probabilistic model.....	7
3. Use of seismic hazard results in risk assessment and decision making.....	11
4. Arguments about mean and fractile hazards.....	14
5. Use of hazard types in NPP regulations.....	15
6. Valorization of the SENSEI hazard results.....	17
6.1 Overview of the SENSEI results	17
6.2 New analyses based on the SENSEI calculations.....	18
7. Discussion and conclusions.....	25
Acknowledgement.....	26
References.....	26
Appendix 1	30
Appendix 2	31

1. Introduction

Probabilistic seismic hazard analysis (PSHA) is a methodology currently used to estimate the probability that the threshold value of the selected earthquake ground-motion measure will be exceeded at the target site or region in a specified time interval. The seminal paper that outlined the methodology dates back several decades (Cornell 1968). PSHA is used in Finland, among many other countries, to provide site-specific input for probabilistic risk assessment (PRA) of nuclear power plants (NPPs).

PSHA is exclusively associated with the vibratory ground motions triggered by natural earthquakes. The so-called secondary earthquake effects, such as tsunamis and landslides or other types of ground failure, are not considered, although they may be the primary cause for devastation. The astronomically expensive catastrophe that impacted the Fukushima Dai-ichi NPPs in eastern Japan in March 2011 was caused by the 24-m tsunami. In Northern Europe, secondary earthquake effects are infrequent, but not unprecedented (Mäntyniemi et al. 2021a). A more detailed list of seismotectonic hazards following the Western European Nuclear Regulators Association (WENRA 2020) is given in Appendix 1.

A complete PSHA integrates a wide range of disciplines (seismology, geology and tectonics, geodesy, statistics, probability theory, uncertainties, and decision theory). Many large-scale PSHA projects, particularly those conducted in the framework of the Senior Seismic Hazard Analysis Committee (SSHAC; Budnitz et al. 1997a, b) emphasize that cognitive psychology also plays a role in making expert judgments. Since the outcomes are input for PRA, structural and geotechnical engineering are involved.

The ground shaking of the moment magnitude **M**5.8 Mineral, Virginia earthquake in the eastern United States on 23 August 2011 caused ground motions at the North Anna NPP that exceeded the plant's safe-shutdown earthquake (SSE) ground motion over a large frequency range (Johnson et al. 2017). This occurrence is in line with the general observation that shaking patterns from relatively moderate earthquakes may be outliers in that they generate more ground shaking than what is expected, based on ground-motion prediction equations (GMPEs) that give the median ground motion. Moderate to large earthquakes are typically of concern for PSHA (Bazzurro and Cornell 1999). For example, **M**5.5 earthquakes are significant sources of strong ground motion (> 0.1 g peak ground acceleration, PGA) at an epicentral distance of 60 km, despite the chance of only 1% of strong ground motion, because **M**5.5 earthquakes occur frequently (Minson et al. 2020). Smaller-magnitude earthquakes may also generate high accelerations that, however, are of short duration. An example is the (body-wave magnitude) m_b 5.0 Ohio earthquake of 31 January 1986 which caused accelerations of 0.18 g at the Perry NPP at a distance of 17 km (Nicholson et al. 1988).

The primary output of PSHAs are hazard curves expressing the annual frequency of exceedance (AFE) of the selected ground-motion measures. When PSHA is performed for design purposes, two decisions must be made to obtain values of ground-motion parameters: which AFE should be adopted, and from which hazard curve should the ground-motion value be read. The current regulatory status in Finland, given in the guide YVL B.7 (2019)(STUK), is that the median confidence seismic hazard at AFE 10^{-5} is used to substantiate the seismic design-basis earthquake (DBE) for NPPs with minimum horizontal PGA value of 0.1 g.

Global examples of exceedance of the DBE ground motion include the Niigataken-Chūetsu-Oki earthquake (**M**6.6) in the Niigata Prefecture of Japan on 16 July 2007. The subsequent ground motion at the site of the Kashiwazaki-Kariwa NPP (KKNPP) exceeded the plant's DBE ground motion by a significant amount, and all seven reactors of the plant were shut down for an extended period (Johnson et al. 2017). The KKNPP units performed well in the situation, but a postearthquake analysis concluded that similar performance cannot be assured for other NPPs given the same loading conditions.

The high variability of shaking patterns from natural earthquakes is evidenced by an **M**6.8 earthquake in the Niigata Prefecture in October 2004 that had no impact on the nearby KKNPP, but an **M**5.2 event there two weeks later caused one of the reactors to trip (World Nuclear Organization WNO). Japan has



experienced several cases in which earthquakes have caused ground motions beyond the DBE levels (Johnson et al. 2017). Prior to 2006, however, they were not considered for study in the country.

The KKNPP restart experience demonstrated the need for formulating specific and detailed criteria for addressing situations in which seismic events trigger ground shaking that exceeds the original design or evaluation basis. The International Atomic Energy Agency (IAEA) provided guidance to operating organizations (IAEA 2011). New definitions of the design basis were implemented in some cases.

The Tōhoku-Oki earthquake of 11 March 2011 was a megathrust event (**M**9.0) that generated very violent ground shaking, moved Honshu Island 3.6 m to the east, shifted Earth's axis by 25 cm, and accelerated its rotation by 1.8 microseconds (Norio et al. 2011). The 11 NPPs in northeastern Japan stopped operating their reactors automatically, and the ground shaking did not significantly damage the safety-related structures, systems, or components of the NPPs (Johnson et al. 2017), but the impact of the tsunami stopped the cooling systems of three of the Fukushima Dai-ichi reactors, which, consequently, led to three core meltdowns.

The earthquake-tsunami induced nuclear crisis drew attention to extreme events and large-scale disaster risks (e.g. Wong 2014), and spurred discussion within the PSHA community (e.g. Geller 2011; Stein et al. 2011; Hanks et al. 2012). One issue is the safety measures based on the scientific knowledge available at the time of construction: how the tsunami hazard is perceived has evolved significantly over the years (Nöggerath et al. 2012). Upgrades were implemented to meet new definitions of the requirements for ground motion beyond that of DBE. The IAEA states that "A set of design extension conditions shall be derived on the basis of engineering judgement, deterministic assessments and probabilistic assessments for the purpose of further improving the safety of the NPP by enhancing the plant's capabilities to withstand, without unacceptable radiological consequences, accidents that are either more severe than design basis accidents or that involve additional failures" (IAEA 2012, 2016). The guide YVL B.7 (2019) states that "exceptional external events and conditions with an estimated frequency of occurrence less than 10^{-5} /year shall be considered design extension conditions (DEC C) events." The memo of the YVL B7 guide states that "In practice, an indicative value would be an acceleration corresponding to the occurrence frequency $1 \cdot 10^{-7}$ /year at the facility site."

The aim of this report is to explore and clarify the association between the seismic hazard and confidence-level results that are relevant to the DBE and the DEC C in Finland. A comparison of interdependences between the DBE and the DEC C is presented. We draw specifically on the outcomes of the SENSEI (SENsitivity study of SEismic hazard prediction in Finland) project conducted under the auspices of STUK in 2019–2020 (Mäntyniemi et al. 2021b; Fülöp et al. 2022). The SENSEI project used national seismicity data and explored the sensitivity of the PSHA output to different choices of input. Its aim was not to produce complete PSHA outcomes to be imposed on by regulations, but instead thoroughly analyzed the different steps of PSHA, which resulted in an extensive set of new PSHA calculations. In addition, the primary outcomes of the CompPSHA coordinated jointly by STUK and the Technical Research Centre of Finland (VTT) in 2015–2018 (OECD 2019) are presented. The CompPSHA project compared PSHA practices in several countries that belong to the Organization for Economic Co-operation and Development (OECD).

First, we outline the PSHA and its consequent use in risk assessment and risk-informed decision-making (sections 2 and 3). We briefly review arguments about the mean and median hazard curves in the PSHA (4), together with summaries of the CompPSHA results (5). We present new figures based on the SENSEI dataset and analyze them (section 6, Appendix 2). We focus on the ratio of the mean and median hazard of PGA, spectral acceleration (SA) at 1 Hz, 5 Hz, and 25 Hz at AFE levels 10^{-4} , 10^{-5} , 10^{-6} , 10^{-7} and 10^{-8} with emphasis on 10^{-5} and 10^{-7} . Finally, we discuss the PSHA state-of-the-art (7).

2. Calculation of seismic hazards using a probabilistic model

Probabilistic modeling of seismic hazards incorporates the aleatory variability inherent in the phenomena (or its representation with a certain model, i.e. apparent aleatory variability) and epistemic uncertainty which constitutes the scientific uncertainty in models of the distributions of earthquake magnitude, location, and ground motion. The terms were introduced to PSHA by Budnitz et al. (1997a, b); however, the epistemic uncertainty has been understood and taken into account over a much longer time (e.g. McGuire 1977, 1993). The contested nature of the separation between the two types of uncertainty and the near impossibility of validating PSHA models makes it difficult to identify and isolate flaws in them (Marzocchi and Jordan 2014).

The intrinsic aleatory variabilities in the PSHA model H_m are included in the exceedance probability calculation as

$$F_m(x) = P(X > x | H_m), \quad \text{Eq. 1}$$

where $F_m(x)$ is the exceedance probability of the ground-motion level X for the specified site, given the intrinsic aleatory variability in the hazard H_m . $F_m(x)$ can be expressed as a seismic hazard curve.

Epistemic uncertainty is handled by assembling a set of alternative PSHA models, each providing a seismic hazard curve. The range of these alternative models covers epistemic uncertainty

$$\{H_{m_i}; m_i \in M\}, \quad \text{Eq. 2}$$

where H_{m_i} is an alternative hazard model, drawn from possible future earthquake scenarios M , based on the best available knowledge of the expert hazard community.

Epistemic uncertainty can, in concept, be reduced by collecting new observations and developing modeling. Improved datasets clearly give reasons for updating PSHA models. In the SENSEI project, new earthquake focal-depth distributions were prepared for northern and southern Finland. The more reliable depth estimates in the 2000s (Uski et al. 2015) follow from an improved detection capability of the Finnish National Seismic Network, dense local seismic networks, and better calculation techniques. However, tailoring detailed, site-specific depth distributions is not an option for the very near future, due to the limited time span of the record and the slow accumulation of new data, particularly in the south of the country.

The various assumptions of the input data can be treated quantitatively, using a logic tree or Monte Carlo analysis (McGuire 1993). The former is a more established state-of-the-art and is considered here. The logic-tree framework was introduced to PSHA by Kulkarni et al. (1984). It is currently standard practice to integrate the designed scenarios of earthquake occurrence into the PSHA in a logic-tree structure. Logic trees serve as tools that capture and quantify the epistemic uncertainty of the seismic source zone and GMPE models (e.g. Bommer et al. 2005). They render it possible to treat probabilistic problems that can be arranged in a hierarchical structure with a discrete number of possibilities (Marzocchi et al. 2015). When PSHA is performed within a logic-tree framework, epistemic uncertainty is expressed in a set of branch weights, by which an expert (group) assigns degree-of-belief values to the applicability of the corresponding branch models. The branch weights are considered subjective estimates for the degree-of-certainty that the corresponding model is the one that should be used (Scherbaum and Kuehn 2011).

If the logic tree covered all the mutually exclusive and completely exhaustive (MECE) and appropriately weighted future earthquake scenarios, the result could be interpreted as the true hazard distribution (Bommer and Scherbaum 2008). However, the MECE conditions are not always fulfilled; for example, input models can be based on shared data, such as different GMPEs relying on the same ground-motion recordings. Thus, PSHA provides an estimate of the future hazard, but opens the possibility for disputes about the best PSHA models and results one among those available (Marzocchi and Jordan 2014).

In practice, logic trees also document and display in a transparent fashion the state of seismotectonic data and knowledge in the target region, since the number of nodes increases with data availability. For

example, the number of fault segments of a mapped active fault that can break in a future earthquake constitute a node with the respective branches. The various rupture lengths lead to different maximum magnitudes associated with the scenarios. Fault mechanisms and other detailed information about the fault behavior can also be included. The number of branches may grow significantly, which makes logic trees computationally demanding. In low-seismicity regions such as the Fennoscandian Shield, by contrast, the corresponding branching typically includes a solitary magnitude distribution that is assumed to protect against all possible vibratory harm from future earthquakes. The main concern is that sufficiently, but not unrealistically high magnitudes are considered. The argumentation can be rather generic, based on global tectonics and lessons learned from geologically and tectonically analogous regions, amended with local considerations (e.g. Koskinen 2013).

Despite the different amounts of data available, there is an epistemic gap at the upper end of the magnitude scale in continental interiors and plate boundaries alike. The largest earthquakes occur here infrequently, and future earthquakes may surprise by the type of rupture, even at plate boundaries. For example, the **M7.3** Landers earthquake in southern California on 28 June 1992 involved the rupture of several surficial and hidden faults over a length of almost 100 km (Hauksson et al. 1993). The Tōhoku-Oki earthquake of 11 March 2011 was a megathrust event not deemed to be possible in eastern Japan (e.g. Wong 2014).

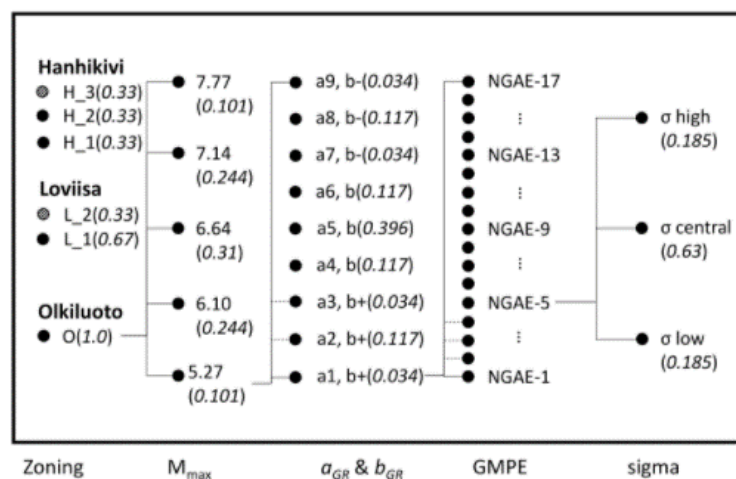


Figure 1. Logic tree for Hanhikivi, Loviisa and Olkiluoto with branching for seismic source zoning, maximum magnitude, the Gutenberg–Richter parameters a and b ($b+$ with standard deviation added and $b-$ subtracted), the ground-motion prediction equation (GMPE) median prediction, and the GMPE randomness (σ) estimate. The GMPE nodes refer to the 17 mean predictions of the Next Generation Attenuation (NGA)-East GMPE, and σ refers to its three ergodic σ models (Goulet et al. 2018, 2021, Youngs et al. 2021). The seismic source zoning models H_3 and L_2 are modifications made during the SENSEI (SENsitivity study of Seismic hazard prediction in Finland) project. The weights of the logic-tree branches are shown, except for the GMPEs which are dependent on the spectral frequency and were taken from Table 9-2 of Goulet et al. (2018). Reproduced from Fülöp et al. (2022).

Figure 1 shows the final logic tree constructed in the SENSEI project with 6885, 4590, and 2295 branches for the sites Hanhikivi, Loviisa, and Olkiluoto, respectively (Fülöp et al. 2022). The numbers are commensurable, since the differences follow from the number of zoning models only. Half of the nodes are associated with the 17 Next Generation Attenuation (NGA) East GMPEs with their respective sigma models. Figure 1 shows the weights of the logic-tree branches, except for the suite of the GMPEs. The weights for each of the 17 GMPEs are dependent on the spectral frequency, as shown in Table 9-2 of Goulet et al. (2018).

Figure 2 illustrates an example of the hazard calculation for Loviisa, based on the logic tree displayed in Figure 1. Clearly, not all logic-tree branches contribute equally to the resulting seismic hazard. GMPE models 11 to 13 contribute little, while models 14 to 17 contribute significantly to the hazard, both at PGA (Fig. 2a) and 1 Hz (Fig. 2b). At PGA, model 10 also contributes significantly, but less so at 1 Hz. Of the

nine different combinations of the a_{GR} and b_{GR} values (which are $a_1 = 1.28/b_1 = 1.2$, $a_2 = 1.08/b_2 = 1.2$, $a_3 = 0.73/b_3 = 1.2$, $a_4 = 1.22/b_4 = 1.07$, $a_5 = 1.04/b_5 = 1.07$, $a_6 = 0.75/b_6 = 1.07$, $a_7 = 1.16/b_7 = 0.93$, $a_8 = 1.0/b_8 = 0.93$, $a_9 = 0.74/b_9 = 0.93$), the last three show the highest concentration of hazard, both at PGA (Fig. 2a) and 1 Hz (Fig. 2b). The interpretation is straightforward: the low b value means relatively more large earthquakes, thus the higher concentration of hazard. The seventh node is the largest contributor at the low and high frequencies shown and has the highest a value associated with the low b value. This illustrates a major challenge of PSHA, namely estimation of the b value for determination of the earthquake occurrence probability for seismic hazard analysis, which justifies the abundant literature on the issue.

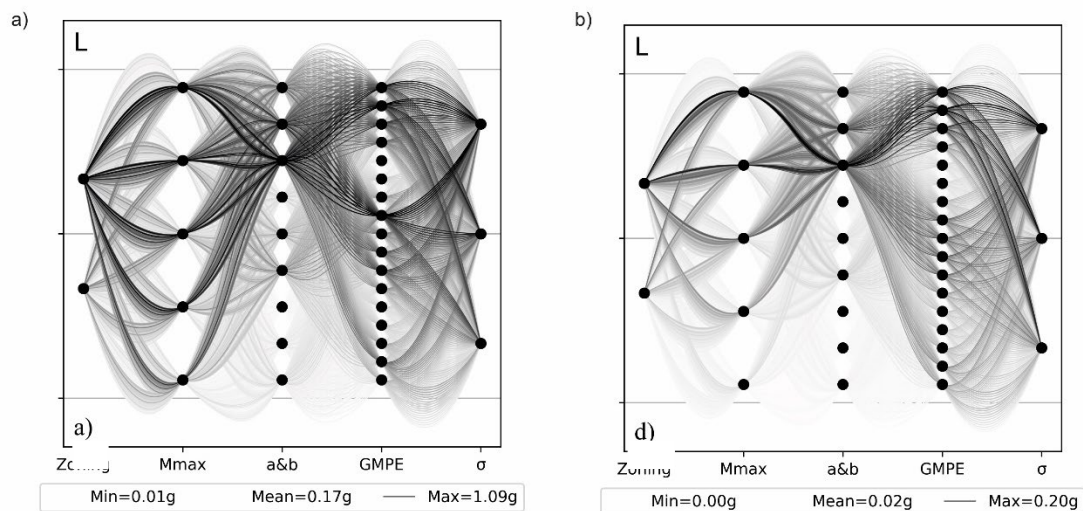


Figure 2. Influence of logic-tree nodes on a) peak-ground acceleration (PGA) and b) 1 Hz-frequency output for annual frequency of exceedance 10^{-5} at the site Loviisa (L). The line tone represents the hazard on the branch normalized to the maximum value of all branches (i.e. the scale is from 0 white to SA_{max}/PGA_{max} black). The minimum, maximum, and mean PGA values are given. Reproduced from Fülöp et al. (2022). The corresponding plots for the other sites can be found in the article. GMPE = ground-motion prediction equation. SA = spectral acceleration.

Figure 3 shows an assembly of hazard curves that represents the output of PSHA for an NPP site in Finland. It shows that the difference between the mean and median hazard is not an issue at higher AFEs that correspond to ordinary residential, commercial, and industrial buildings, but the difference grows with AFE 10^{-4} and lower relevant to critical infrastructure. At AFE 10^{-5} , the mean hazard curve is closer to the median than to the 84th percentile, and at AFE 10^{-6} it is approximately between them. At AFE 10^{-7} , the mean is closer to the 84th percentile than to the median, and it continues to approach the 84th percentile until the lowest AFE shown (10^{-9}).

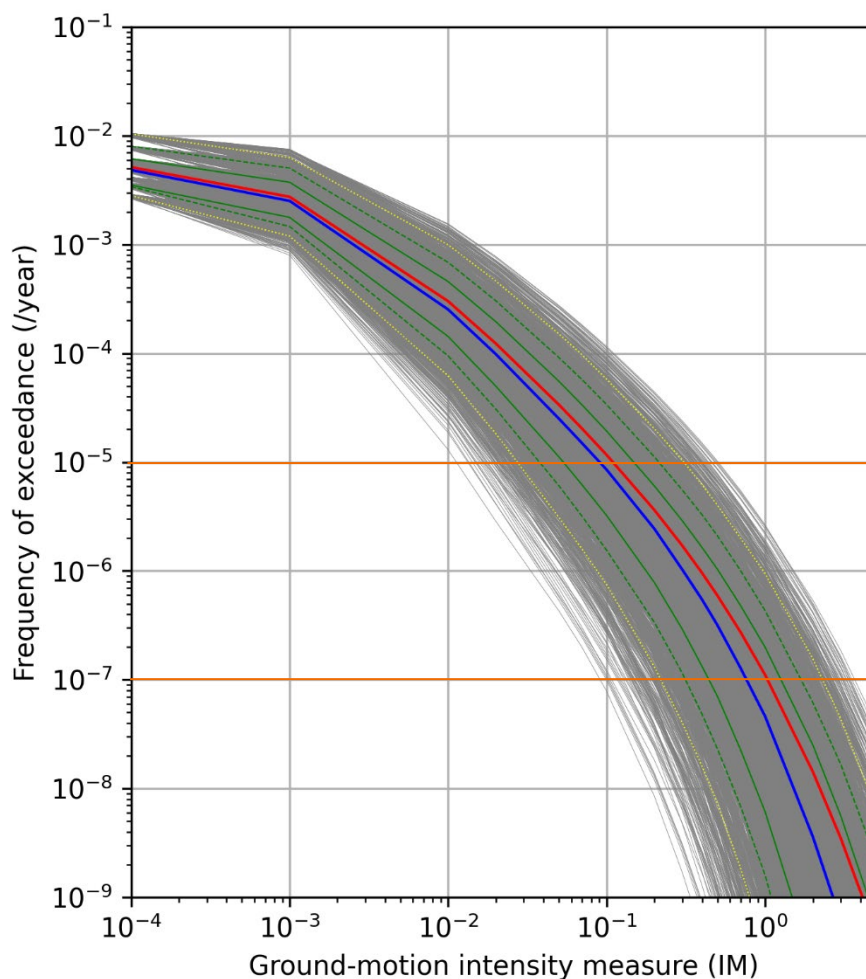


Figure 3. An example of seismic hazard curves for a nuclear power plant (NPP) site in Finland. The spread of the gray lines covers the epistemic uncertainty range. The mean hazard is plotted with a continuous red line and the median with a continuous blue line. The yellow lines are the 1% and 99%, green dashed lines the 5% and 95%, and green continuous lines the 16% and 84% percentile hazard curves. Annual frequencies of exceedance 10^{-5} and 10^{-7} are highlighted by the light brown horizontal lines.

In December 2021, the European Seismic Hazard Map 20 (ESHM20) was released with the main outcome of PSH maps for mean return periods of 50, 475, 975, 2500, and 5000 years (Danciu et al. 2021). The ESHM20 hazard curves and uniform hazard spectra (UHS) at every location of the computational grid covering Europe were calculated for the mean, median, and four quantiles (5th, 16th, 84th, 95th). The PGA mean values for a 10% probability of exceedance in 50 years, corresponding to a mean return period of 475 years, are a standard outcome of interest for general building codes, and not directly usable to the present considerations. However, such large-scale initiatives are important incentives for development of the methodology used. In their review of the state-of-the-art PSHA, Gerstenberger et al. (2020) focused on quantifying and reducing the reducible uncertainties of seismic hazard mapping at national scales. They considered future directions to be a better quantification of the uncertainties in the knowledge of earthquake processes.

3. Use of seismic hazard results in risk assessment and decision making

Hazard curves must be placed into the context of their practical application. In the nuclear context, they serve as input for further assessment of earthquake consequences and risk. Such further assessment is divided into deterministic and probabilistic. It can take place in the framework of performance-based assessment (PBA) (Cornell and Krawinkler 2000, Deierlein and Moehle 2004, Krawinkler and Miranda 2004). The PBA methodology integrates four levels of uncertainties related to consequences of earthquake exposure. These uncertainties are integrated in PBA by means of random variables for earthquake intensity measures, engineering demand parameter, damage measure, and a so-called decision variable (e.g. Zareian and Krawinkler 2012).

The ground-motion intensity measure (IM) is the main output of the hazard analysis (such as peak-ground acceleration, period T spectral response SA(T)), the engineering demand parameter (EDP) is a measure of the structural response, such as floor displacement or floor acceleration, the damage measure (DM) quantifies probabilistically the level of expected damage of individual components (e.g. damage state of shear walls i) and the decision variable (DV) described the performance of the building (e.g. by % loss of value). PBA links the earthquake intensity measures, from the hazard domain to the engineering demand parameter and/or component/structure fragilities, in the structural system domain and further to loss estimates.

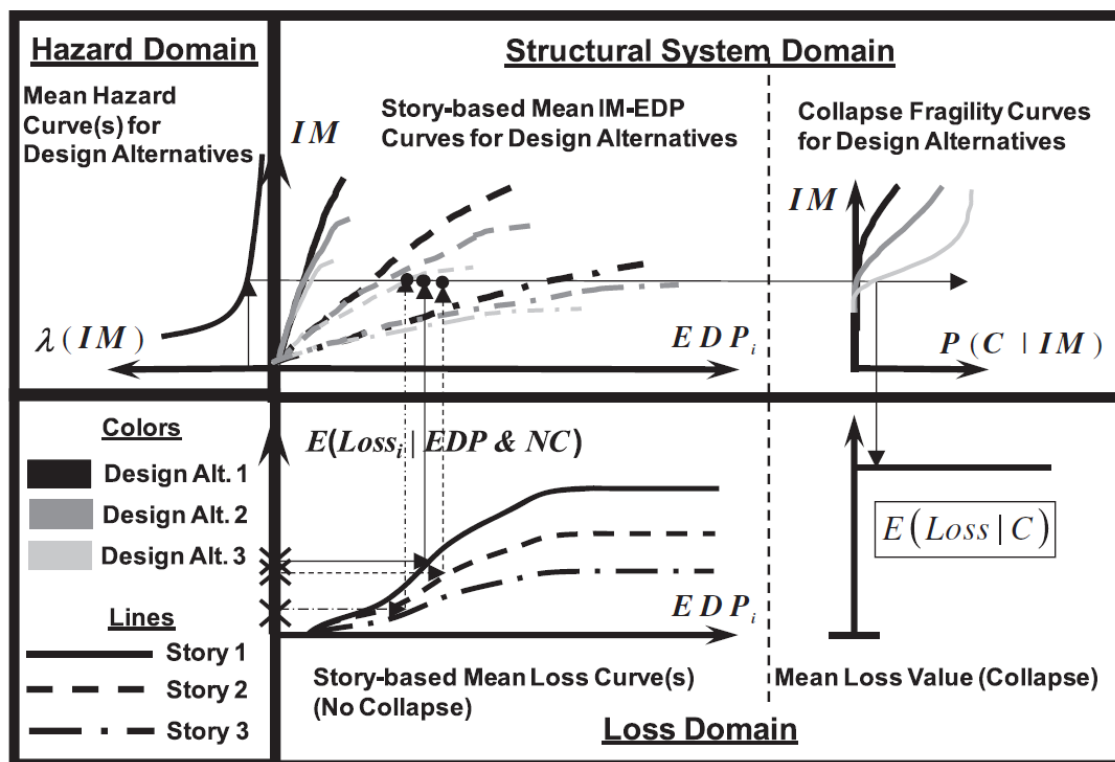


Figure 4. Schematic representation of the calculation process in performance-based assessment (PBA). The intensity measures (IMs) and their frequencies of exceedance $\lambda(IM)$ are calculated by PSHA in the hazard domain. The IMs are linked with engineering demand parameters (EDP) and component fragilities and losses. Reproduced from Zareian and Krawinkler (2012).

The scheme in Figure 4 presents the comparative evaluation of three design alternatives for a 4-storey structure. The mean hazard (IM) is identified from the hazard curves for the target AFE (i.e. $\lambda(IM)$ axis on the left). A suite of ground motions compatible with this IM is selected and used to calculate the engineering demands (EDPs), such as the acceleration at each floor level. Since multiple ground motions are used and the structural models may also incorporate randomness (e.g. geometric dimensions, distribution of material strength), the IM to EPD relationship also includes randomness. The mean IM to EPD relationship

is meant to be used (central column of Figure 4) to estimate the losses on each floor. The mean value of the loss-curves is employed for the storey-based losses. In addition, the collapse of the building and associated loss can be estimated using fragility curves associated with the collapse of the structure (the right side of Figure 4).

The same conceptual framework can be used to evaluate NPP safety by seismic probabilistic risk analysis (SPRA). SPRA is a method to compute the seismic risk by means of annual frequency of unacceptable performance of the plant. This is achieved by integrating the seismic hazard (i.e. hazard curves) with the plant fragility data over a wide range of IM levels. SPRA incorporates the entire range of uncertainties in seismic hazard, structural response, and properties/capacities of NPP components. The general procedure is presented by Huang et al. (2011), among others, and is exemplified in Figure 5. Figure 5a expresses the mean core-melt fragility (conceptually comparable with the collapse-fragility from Figure 4), and Figure 5b is the peak-ground acceleration hazard curve (the same as in Figure 4). The mean/average core melt probability for PGA in the range of 0.45–0.55 g is approximately 0.5, and the annual frequency of PGA between these two limits is about 0.0011. Hence, $0.5 \cdot 0.0011$ represents the annual frequency of core melt contributed by the range of PGA between 0.45 g and 0.55 g, and the contributions from all PGAs can be calculated by summing/integrating the entire range of PGAs (Huang et al. 2011).

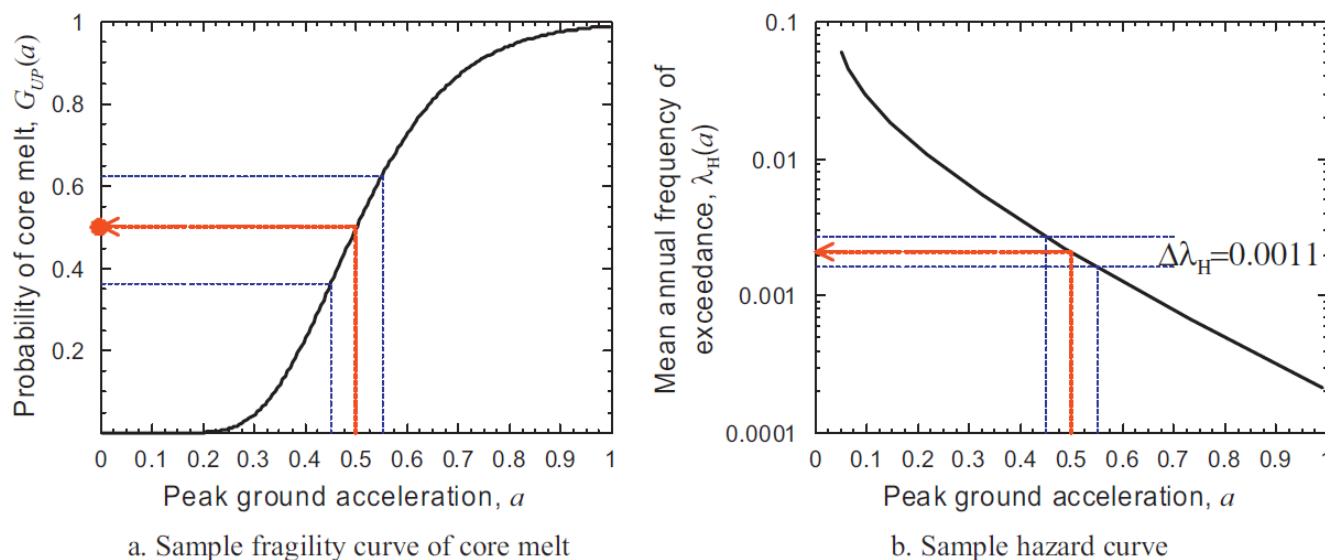


Figure 5. Generic mean core-melt fragility curve and mean hazard curve. The x-axis is commonly the peak-ground acceleration (PGA) at the site. Reproduced from Huang et al. (2011).

The summation, or integration, over the entire range of PGAs is written as the risk equation (Huang et al. 2011) as follows:

$$\lambda_{UP} = \int G_{UP}(a) \left| \frac{d\lambda_H(a)}{da} \right| da, \quad \text{Eq. 3}$$

where λ_{UP} represents the annual frequency of unacceptable performance, $G_{UP}(a)$ is the conditional probability of unacceptable performance, given the value of ground motion intensity a and can be read from the fragility curve. $\lambda_H(a)$ is the probability of ground motion intensity a , read from the hazard curve.

When single values of the hazard and fragility are used, the preferred values are the expected ones, i.e. mean hazard and fragility. The integration can be carried out using multiple hazard and fragility curves, accounting for the uncertainties of hazard and fragility. The hazard distribution can be represented by i equally weighted hazard curves, each with $P_{H(i)}$ weight, and the core melt fragility by j equally weighted fragility curves, each weighted $P_{F(j)}$. In order to represent the entire hazard and fragility space, $i \times P_{H(i)} = 1$ and $j \times P_{F(j)} = 1$, and the risk equation can be written as



$$\lambda_{UP} = \sum_i \sum_j P_{H(i)} \times P_{F(j)} \times \int G_{UP(j)}(a) \left| \frac{d\lambda_{H(i)}(a)}{da} \right| da, \quad \text{Eq. 4}$$

where $P_{H(i)}$ and $P_{F(j)}$ are the weights of the i^{th} hazard and j^{th} fragility curve respectively, $G_{UP(j)}(a)$ is the conditional probability of unacceptable performance on the j^{th} fragility curve, given the value of ground motion intensity a , and $\lambda_{H(i)}(a)$ is the probability of ground motion intensity of the i^{th} hazard curve.

4. Arguments about mean and fractile hazards

As discussed in section 2, global and regional seismic hazard mapping is not directly relevant to our current considerations, since its key outcome is typically the horizontal PGA for a mean return period of 475 years. Nevertheless, large-scale hazard-mapping projects act as important spurs for the development and harmonization of PSHA practices. For example, preparation of the first global seismic hazard map in the 1990s (Giardini and Basham 1993) significantly increased the standardization of PSHA practices and cross-border cooperation worldwide. The calculation was on mean hazard results (Basham and Giardini 1993). McGuire (1993) emphasized that the ranges of hazards should be represented by including several fractiles and the mean hazard to allow risk-mitigation decision-making to consider uncertainties in an appropriate manner. If a single result is needed, the mean should be selected, primarily because it is sensitive to all scenarios, including the extreme scenarios that drive the hazard at low AFEs. McGuire (1993) also argued that, in the decision-theoretic sense, the mean hazard allows target safety goals to be met over all sites.

An exception to the prevalent rule of the mean hazard curve for engineering design was presented by Abrahamson and Bommer (2005). Their opinion note focused on low AFEs and was motivated by the need for critical infrastructure (NPPs in Switzerland in the Probabilistic Seismic Hazards Analysis for Swiss Nuclear Power Plant Sites (PEGASOS) project, Abrahamson et al. 2004; a possible repository for spent nuclear fuel and high-level radioactive waste at Yucca Mountain, Nevada, USA, Stepp et al. 2001). They remarked on the mean hazard curve increasing over high fractiles at low AFEs (this behavior is shown in Figure 3 on pages 9–10) and that it results in very high ground motions to be considered, although they admitted that it is not alone a valid reason for adopting a different hazard curve. They based their argumentation on the interpretation of the branch weights (which in their view are confidence levels rather than probabilities) and on the instability of the mean hazard curve.

In their reply opinion, McGuire et al. (2005) concluded that it is preferable to use the mean from the risk point of view. One of their arguments relates to the widespread distinction used in PSHA, namely aleatory variability (inherent randomness of a process) and epistemic uncertainty (due to limited knowledge). McGuire et al. (2005) listed cases in which the distinction was not a trivial one to make, so any expert judgment made would influence the median hazard. Risk-mitigation decisions are often not influenced by the source of the uncertainty in hazards. The second set of arguments relates to the use of mean hazard in risk calculations and the ease of combining the consequences of seismic hazard with other types of hazards (such as those from strong winds). McGuire et al. (2005) concluded that the use of mean hazard is consistent with modern interpretations of probability and with precedents of safety goals and cost-benefit analysis. McGuire et al. (2005) pointed out that it is inappropriate to perform a PSHA with implausible interpretations, and then choose as a hazard measure a fractile that is insensitive to these interpretations. Instead, the implausible interpretations should be screened out from the PSHA model itself, or weighted with low weights. Deliberately choosing median as a hazard measure may result in powerless decisions, since extreme scenarios would be disregarded.

Musson (2005) argued against the use of fractiles that are representations of single hazard curves and whose usage would result in abandoning the idea of probabilism. The probability that all conditions in the single branch of the logic tree that the curve represents are true is very small. Each fractile represents a state of epistemic uncertainty.

Clearly, the use of fractiles or the mean can differ outside the task of engineering design. As discussed in section 2, validation of PSHA models is a challenge, whereas comparison of models is a basic task to conduct after a new model becomes available. Different models should not be compared only by use of the mean.

5. Use of hazard types in NPP regulations

STUK and VTT jointly coordinated the CompPSHA project in 2015–2018 (OECD 2019; Okko et al. 2019). STUK collected information about up-to-date PSHA practices in the OECD member countries, using a questionnaire sent to the representatives of countries participating in the OECD, Nuclear Energy Agency (NEA) and Working Group on Integrity and Ageing of Components and Structures (WGIAGE). The questionnaire concerned details of PSHA practices in the nuclear field, such as assisting criteria, data collection and PSHA method, seismic source zones, logic trees, GMPE, ground condition, treatment of uncertainties, as well as PSHA outputs and the use of them. The following countries provided answers: Belgium (BE), Canada (CA), the Czech Republic (CZ), Finland (FI), France (FR), Germany (DE), Japan (JP), the Netherlands (NL), South Korea (KR), Spain (ES), Sweden (SE), Switzerland (CH), and the United Kingdom (UK). The respondent countries are situated in different tectonic environments; e.g. Japan is a high-seismicity country at a plate boundary, whereas eastern Canada is situated in plate interiors and is comparable to Finland in many ways.

As expected, the main use of PSHA outputs is for structural response analysis and soil-structure interaction analysis. The interface between seismology and earthquake engineering was typically reported to be PGA and the UHS. Outputs are usually specified in terms of UHS, reporting a few spectral frequency values alongside the PGA. The UHS is presented down to low AFEs, depending on the seismicity of the sites, i.e. to AFE 10^{-7} (CH), 10^{-6} (JP, BE), 10^{-5} (DE), 10^{-9} (FI – cf. Figure 3). A very detailed PSHA output was given by Switzerland (CH), where the results for mean, median, and the 5th, 16th, 84th, and 95th fractile hazard curves were reported at different levels in the soil profile, including (1) free-field, (2) foundation level, and (3) base-rock level. At the time of the survey, Switzerland was the only country in Europe to have carried out an SSHAC Level 4 PSHA project (Abrahamson et al. 2004).

The hazard results reported by nine respondent member countries are listed in Table 1 (reproduced from the OECD report of 2019). Some differences exist within individual countries with respect to different NPP units (UK), or the level of seismicity expected (FR). In general, the SSE of the equivalent earthquake level was reported.

The frequency assumed for PGA ranges from 20 Hz (NL) to 100 Hz (BE, FI, CH). This parameter, along with the frequency for the PSA spectral peak, is dependent on the soil conditions. NPPs in Finland are situated on very hard rock and are characterized by a higher frequency for PGA (i.e. 100 Hz) and the spectral peak (i.e., 10 Hz). Only Sweden uses a higher frequency for the spectral peak location at 20 Hz.

The SSE-level PGA ranges from 0.05 g (FR-low) to 0.39 g (CH). The so-called spectral amplification, the ratio between the peak of the spectral response and PGA ($PSA_{\max 5\%} / PGA_{\text{SSE}}$), is between 1.8 and 4.4. The two columns on the right of Table 1 list the hazard component (mean or median) and the AFE used for the definition of SSE. The most common choice among these nine countries is the mean hazard at either AFE 10^{-4} or 10^{-5} .



Table 1. Main features of UHS developed by PSHA in nine OECD member countries (reproduced from Table 6 of OECD 2019).

	Reactor	Freq. for PGA (Hz)	Location of PSA spectra peak (Hz)	PGA _{SSE} (m/s ²)	PSA _{max5%} (m/s ²)	PSA _{max5%} / PGA _{SSE}	Hazard curve	AFE/SSE
BE		100	10	0.99/ 1.04	2.27/ 2.38	2.3/ 2.3	mean	10 ⁻⁴
		100	10	1.39	3.21	2.3	mean	10 ⁻⁴
FI	4	50	10	1	2.3	2.3	median	10 ⁻⁵
FR	Low	100	5	0.5	1.26	2.5		
	Mid	100	5	1	2.47	2.5		
	High	100	5	1.5	3.66	2.4		
DE	North	33	4.5	1.2	3.5	2.9	84%	10 ⁻⁵
	South	33	2.5	0.75	2.34	3.1	median	10 ⁻⁵
ES	-	-	-	-	-	-	-	10 ⁻⁴ –10 ⁻⁵
NL	All	20	1	0.6	1.1	1.8	-	10 ⁻⁴
SE	10	50	20	1.1	3.7	3.4	-	10 ⁻⁵
CH	Bez	100	5	3	7.9	2.6	mean ^f	10 ⁻⁴
	Müh	100	10	3.6	8.5	2.4	mean ^f	10 ⁻⁴
	Gös	100	5	3.9	11.3	2.9	mean ^f	10 ⁻⁴
	Lei	100	5	3.6	10.9	3.0	mean ^f	10 ⁻⁴
UK	1	40	5.3	1.4	4.2	3.0	mean	10 ⁻³ (two diverse lines of reactor protection)
	2	40	5.3	1.4	4.2	3.0	mean	
	3	40	1.8/2.5	2.5	7.4/11	4.1/ 4.4	mean	
	4	40	1.8/2.5	2.5	7.4/11	4.1/ 4.4	mean	
	5	40	6	1.4	3.1	2.2	mean	10 ⁻³ (single line of reactor protection)
	6	40	6	2.1	5.2	2.5	mean	
	7	40	13	2.3	5.2	2.3	mean	
	8	40	6	1.7	4.2	2.5	mean	

Note: ^f stands for foundation-level hazard

UHS = uniform hazard spectra, PSHA = probabilistic seismic hazard analysis, OECD = Organization for Economic Cooperation and Development, PGA = peak-ground acceleration, SSE = safe-shutdown earthquake, AFE = annual frequency of exceedance, AFE/SSE = AFE used for defining SSE, PSA_{max5%} = peak spectral response, PGA_{SSE} = SSE-level PGA, PSA_{max5%} / PGA_{SSE} = spectral amplification

6. Valorization of the SENSEI hazard results

We first give a snapshot of the SENSEI results and then present new analyses based on the SENSEI set of hazard calculations.

6.1 Overview of the SENSEI results

The SENSEI project aimed at exploring the sensitivity of the PSHA models. The hazard computations were based on so-called pruned logic trees, in which only the host seismic hazard zones and the second most contributing contiguous zones were included for each site (further details on the pruning process can be found in Fülöp et al. 2022). The median and mean hazards generated for the three nuclear sites in Finland are the basis for the analysis given below.

Figure 6 illustrates the mean and median hazard curves of the spectral frequencies of 1 Hz, 5 Hz, 25 Hz, and PGA at the target sites Hanhikivi (H), Loviisa (L), and Olkiluoto (O). It shows how the mean hazard exceeds the median hazard in all cases. This is expected, because peak-ground-motion parameters, such as the PGA, are generally assumed to follow the lognormal distribution, for which the mean is larger than the median, due to the skewness of the distribution. The spectral amplitude (SA) at 5 Hz is approximately equal to the PGA amplitude. The 25-Hz amplitude is above the PGA amplitude, whereas the 1-Hz spectral amplitude is below it.

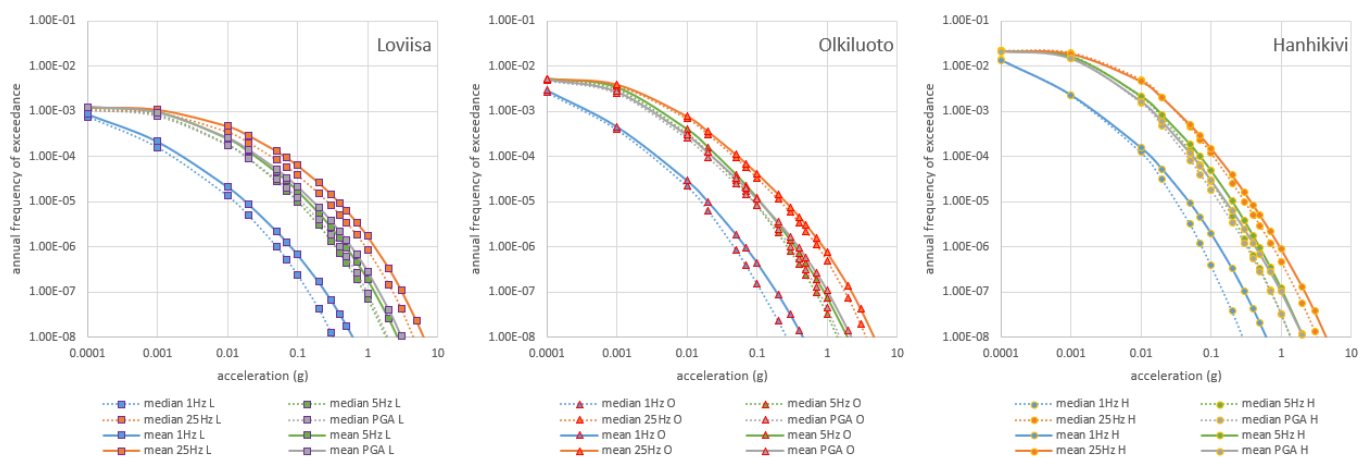


Figure 6. Median (dashed line) and mean (solid line) hazard curves for 1 Hz (blue), 5 Hz (green), 25 Hz (orange), and PGA (gray) at Loviisa (L, purple square), Olkiluoto (O, red triangle), and Hanhikivi, (H, yellow circle).

The mean and median SAs at AFE 10^{-5} are given in Figure 7 for the spectral frequencies of 1 Hz, 5 Hz, 25 Hz, and PGA (100 Hz) selected in the SENSEI project and a more extensive set of values available for the NGA-East suite of GMPEs (Goulet et al. 2018, 2021; Youngs et al. 2021). The general shapes of the mean and median spectra are similar and peak in the range of 20–25 Hz. Mean spectra always exceeded the median spectra, and the difference between them appears fairly pronounced, due to the linear-scale vertical axis. The largest apparent difference between mean and median is seen in Loviisa and the smallest in Olkiluoto. The largest difference between the selected frequencies and the more complete number appears at Hanhikivi, suggesting that the choice of four frequencies was not sufficient for the site.

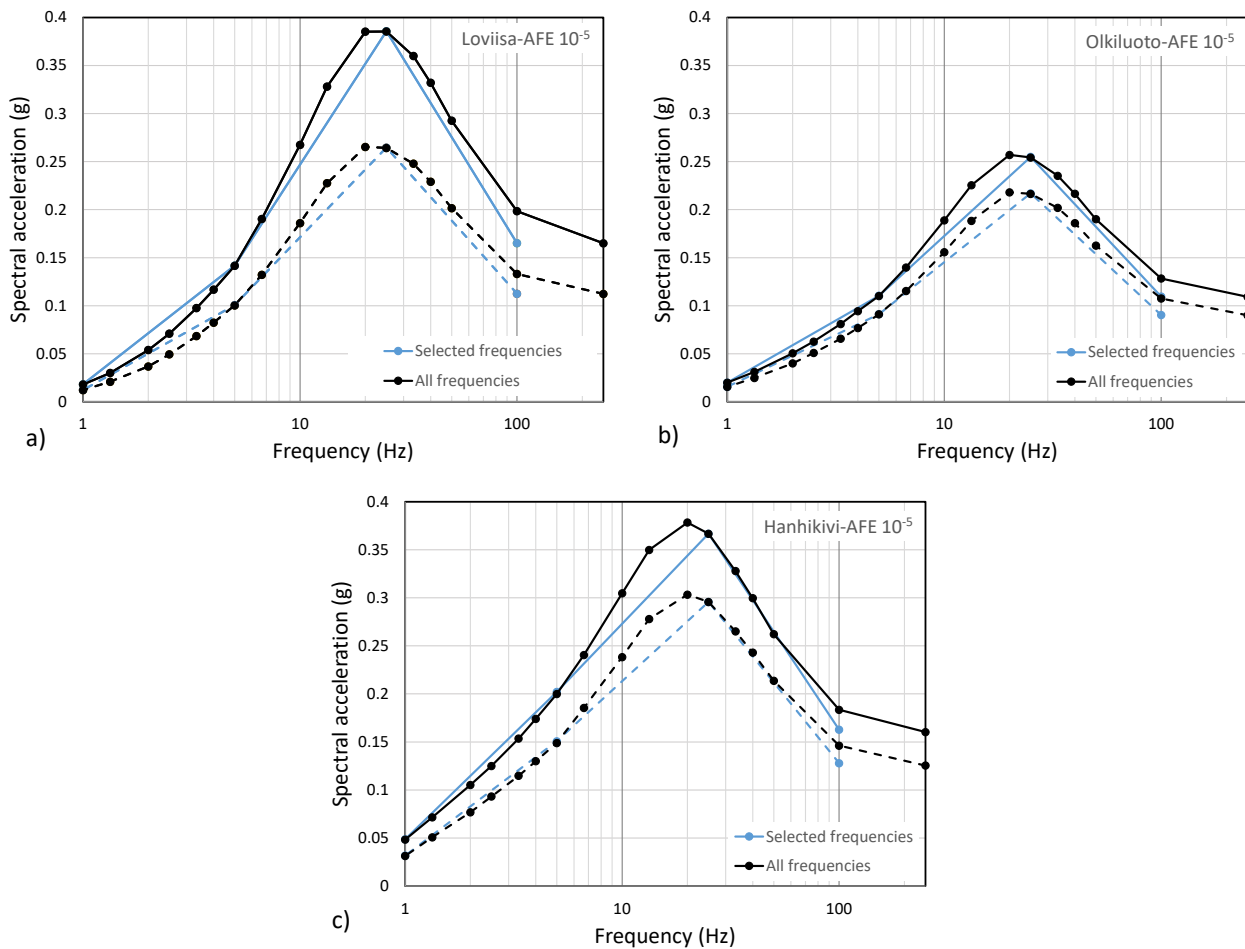


Figure 7. Spectral shape for the sites (a) Loviisa, (b) Olkiluoto and (c) Hanhikivi. The mean spectra are shown with continuous lines, and the median spectra with dashed lines. The spectra with all (black) frequencies available in the NGA-East and selected SENSEI calculation frequencies (blue) are shown. Note that the vertical axis is linear.

6.2 New analyses based on the SENSEI calculations

More complete representations of the individual hazard curves for PGA and SA(1Hz) are given in Figure 8. It shows that the mean estimate is very close to the median at higher AFEs. However, at lower AFEs the mean shifts towards the 84th percentile curves and for Hanhikivi 1 Hz the mean exceeds the 84th percentile at extremely low AFE. This behavior is also illustrated in Figure 3.

The range of the hazard estimates is broadest at Loviisa for PGA and at Hanhikivi for 1 Hz. This may follow from the use of two seismic source zonings for Loviisa and three for Hanhikivi and a single zoning for Olkiluoto. Zoning and the Gutenberg-Richter parameters were explored in SENSEI only in a limited way, without an access to the original earthquake catalogs.

Because of the very low PGA value 0.0001 g, the hazard curves converge to the total activity level of the zones included in the models, because any earthquake will generate such small accelerations. The convergence of the hazard curves to a constant level for low acceleration can also be seen in Figure 6. Hence, the uncertainties at 0.0001 g PGA can be attributed to the effects of the zoning and Gutenberg-Richter parameters. The GMPEs do not contribute to uncertainty at low PGA. For higher values of the PGA, however, the uncertainties of zoning and GMPE add up.

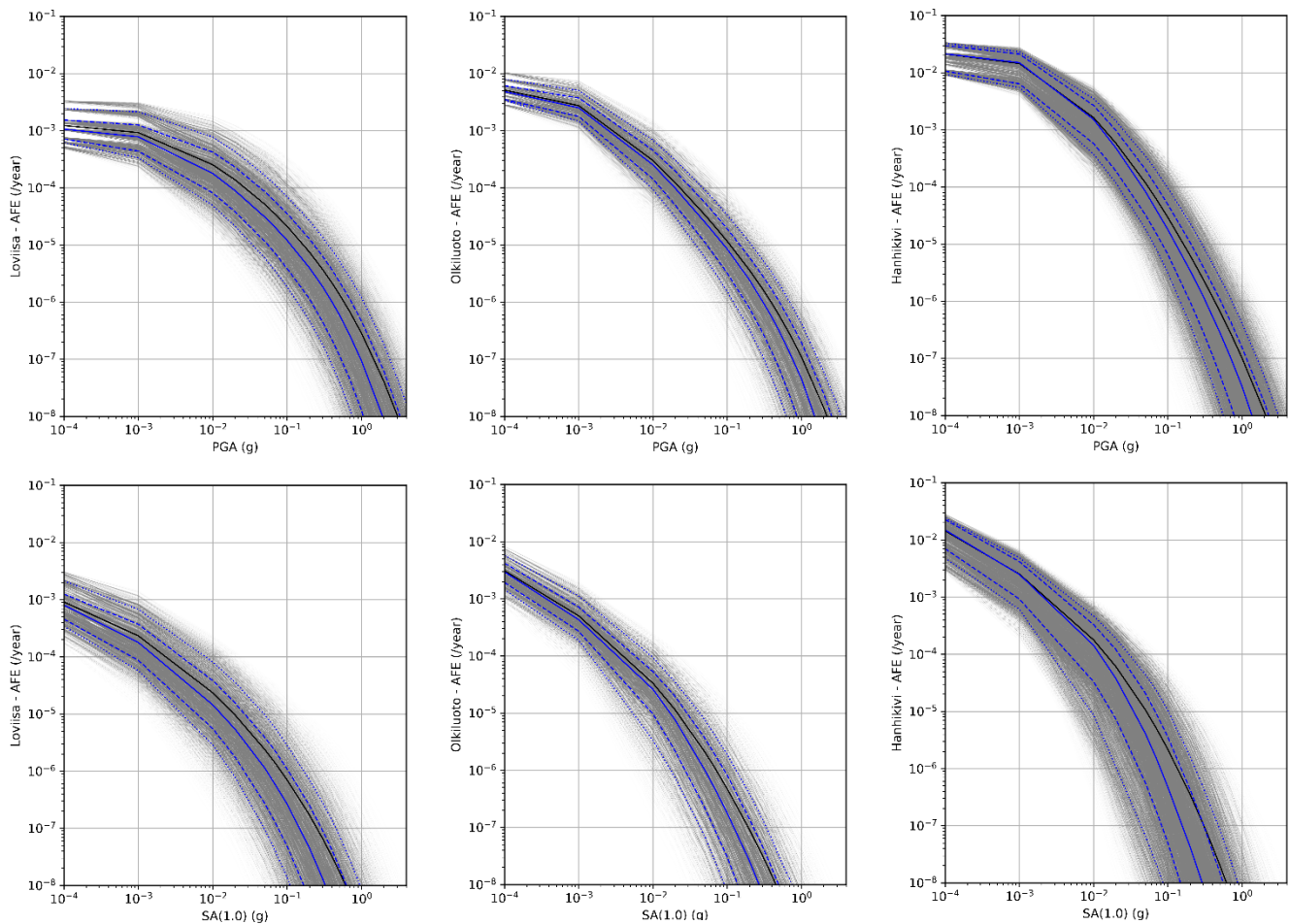


Figure 8. Range of hazard for the sites of (a) Loviisa, (b) Olkiluoto and (c) Hanhikivi for PGA and a representative low frequency (1Hz). The gray lines are the individual hazard curves, with intensity depending on the weight of the logic-tree branch producing them. Hence the more extreme (i.e. low and high) estimates are less visible. The black line is the mean, the continuous blue the median hazard. The dashed blue lines are 16th and 84th and the dotted blue lines the 5th and 95th percentile bounds.

Properties of the distribution of AFEs were extracted for PGA 0.0001 g, 0.01 g and 0.1 g from the data of Figure 8. They can be interpreted as vertical cuts within Figure 8. The characteristics of the distribution are given in Table 2. The interesting quantities to monitor are the ratio of mean to median AFE for the same PGA intensity. As expected, the mean AFE is higher, and the difference increases with increasing PGAs. The coefficient of variation (COV, i.e. the ratio of standard deviation and mean) also increases with increasing PGAs, and the earlier noted trend that dispersion of the results is highest for Loviisa is quantified now, with larger COV for this site. In addition, the Loviisa COV is larger for PGA 0.0001 g, which points at zonation as the source of the dispersion.



Table 2. Properties of the AFE distribution at PGA 0.0001, 0.01 and 0.1 for the three sites.

Site	PGA(g)	Median AFE	Mean AFE	STD	COV	Mean AFE /Median AFE
Loviisa	0.0001	1.06E-03	1.23E-03	6.47E-04	0.53	1.16
	0.01	1.79E-04	2.54E-04	2.31E-04	0.91	1.42
	0.1	1.21E-05	2.13E-05	2.77E-05	1.30	1.76
Olkiluoto	0.0001	4.84E-03	5.14E-03	1.67E-03	0.32	1.06
	0.01	2.53E-04	3.01E-04	1.92E-04	0.64	1.19
	0.1	8.52E-06	1.16E-05	1.13E-05	0.97	1.37
Hanhikivi	0.0001	2.13E-02	2.13E-02	8.17E-03	0.38	1.00
	0.01	1.52E-03	1.64E-03	1.01E-03	0.62	1.08
	0.1	1.80E-05	2.95E-05	3.37E-05	1.14	1.64

Table 3 shows the ratio of the AFE 10^{-7} and AFE 10^{-5} spectral amplitude in terms of median and mean confidence. These numbers indicate how many times the hazard is larger at AFE 10^{-7} in comparison with AFE 10^{-5} . The ratios are in the range of 4.8–14. They are highest for low frequencies at Loviisa and lowest for low frequencies at Hanhikivi.

Table 3. Ratio of intensity measure (IM) at AFE 10^{-7} and AFE 10^{-5} for the three sites.

Site	Hazard component	IM _{AFE 10-7} / IM _{AFE 10-5}			
		PGA	25Hz	5Hz	1Hz
Loviisa	Mean	8.8	8.1	8.8	13.9
	Median	8.7	8.6	8.8	11.7
Olkiluoto	Mean	9.5	8.8	8.2	9.5
	Median	8.4	8.3	7.6	7.6
Hanhikivi	Mean	6.2	6.0	5.2	6.2
	Median	5.5	7.4	4.8	4.7

Table 4 and Figure 9 present the ratios of SA_{mean} to SA_{median} for the three sites. As expected, the mean hazard exceeds the median hazard, since many of the underlying distributions of the PSHA model have long tails toward larger values. The ratios range from 1.14 to 2.17. The highest ratios are reached at lower frequencies (especially 1 Hz). Loviisa (L) has generally higher ratios than Hanhikivi (H) and Olkiluoto (O). For example, the mean PGA values for AFE 10^{-5} are 28%, 47%, and 21% higher than the median values for Hanhikivi, Loviisa, and Olkiluoto, respectively.

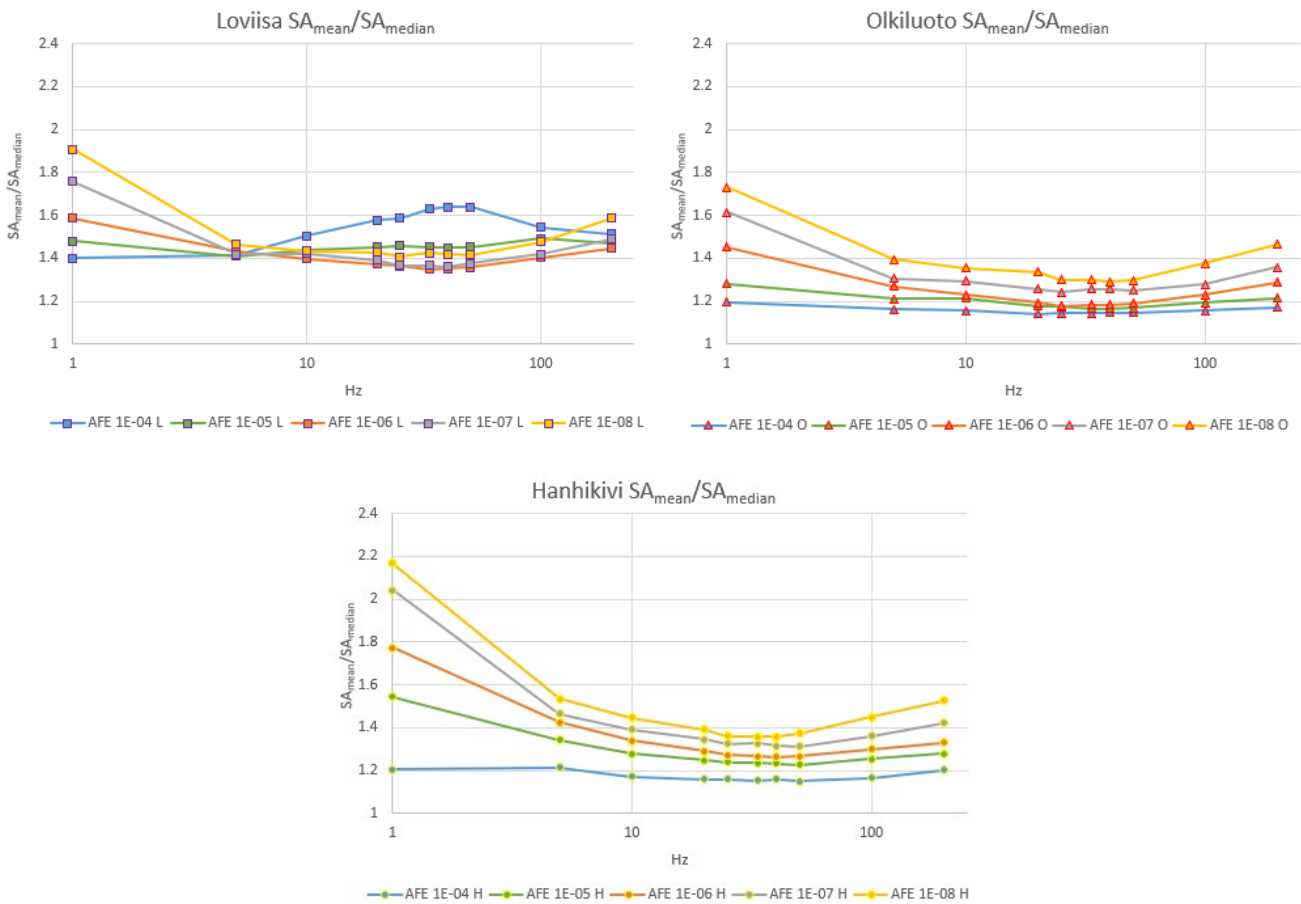


Figure 9. Ratio of mean and median spectral acceleration at the Loviisa, Olkiluoto and Hanhikivi sites for annual frequencies of exceedance 10^{-4} to 10^{-8} . Peak ground acceleration values are plotted at 200 Hz.

Table 4. Hazard spectral ratios SA_{mean}/SA_{median} for Loviisa (L), Olkiluoto (O) and Hanhikivi (H) for frequencies 1Hz, 5Hz, 10Hz, 20Hz, 25Hz, 33.33Hz, 40Hz, 50Hz, 100Hz, and PGA at AFE levels 10^{-4} to 10^{-8} .

	1Hz	5Hz	10Hz	20Hz	25Hz	33.33Hz	40Hz	50Hz	100Hz	PGA
AFE 1E-04 L	1.40	1.41	1.50	1.58	1.59	1.63	1.64	1.64	1.54	1.51
AFE 1E-05 L	1.48	1.41	1.44	1.45	1.46	1.45	1.45	1.45	1.49	1.47
AFE 1E-06 L	1.59	1.43	1.40	1.37	1.36	1.35	1.35	1.36	1.40	1.45
AFE 1E-07 L	1.76	1.42	1.42	1.39	1.37	1.37	1.36	1.38	1.42	1.49
AFE 1E-08 L	1.91	1.47	1.43	1.43	1.41	1.42	1.42	1.41	1.48	1.59
AFE 1E-04 O	1.20	1.16	1.16	1.14	1.14	1.14	1.15	1.15	1.16	1.17
AFE 1E-05 O	1.28	1.21	1.21	1.18	1.18	1.17	1.16	1.17	1.19	1.21
AFE 1E-06 O	1.45	1.27	1.23	1.19	1.18	1.18	1.18	1.19	1.23	1.29
AFE 1E-07 O	1.61	1.31	1.29	1.26	1.24	1.26	1.26	1.25	1.28	1.36
AFE 1E-08 O	1.73	1.40	1.36	1.34	1.30	1.30	1.29	1.30	1.38	1.46
AFE 1E-04 H	1.21	1.21	1.17	1.16	1.16	1.15	1.16	1.15	1.16	1.20
AFE 1E-05 H	1.54	1.34	1.28	1.25	1.24	1.24	1.23	1.23	1.26	1.28
AFE 1E-06 H	1.77	1.42	1.34	1.29	1.27	1.27	1.26	1.27	1.30	1.33
AFE 1E-07 H	2.04	1.46	1.39	1.34	1.32	1.33	1.32	1.31	1.36	1.42
AFE 1E-08 H	2.17	1.54	1.45	1.39	1.36	1.36	1.36	1.37	1.45	1.53



Table 4 shows that the ratios increase with decreasing AFE. This is expected, because the distribution of the hazard curves broadens with decreasing AFE, as the forecast for such low probabilities becomes more uncertain. The broader distribution also means larger difference between median and mean.

A shift from AFE 10^{-5} median hazard for DBE to AFE 10^{-5} mean hazard would result in an increase of 1.23 to 1.54 times the hazard for Hanhikivi, with respective increases of 1.41 to 1.49 times for Loviisa and 1.16 to 1.28 times for Olkiluoto. The DEC C definition to be changed from AFE 10^{-7} median to mean would result in an even larger increase: 1.31 to 2.04 times for Hanhikivi, 1.36 to 1.76 times for Loviisa and 1.24 to 1.61 times for Olkiluoto.

The converses of the above, the AFE for mean and median, are explored in the following. The ratios of AFE_{mean} and AFE_{median} for different spectral acceleration levels (0.001g, 0.01g, 0.05g, 0.1g, 0.2g, and 0.3g) are shown in Figure 10 and Table 5.

The ratios range from 0.95 to 12.81 and differ between the sites. While Hanhikivi has much higher ratios than the other two sites, starting from 0.05g, it has the smallest ratios for accelerations below 0.01g. For example, the mean AFE levels for acceleration 0.1g for PGA are 64%, 76%, and 37% higher than the median AFE levels for Hanhikivi, Loviisa, and Olkiluoto, respectively. The much higher ratios for 1Hz are clear; however, it is not evident what causes this effect.

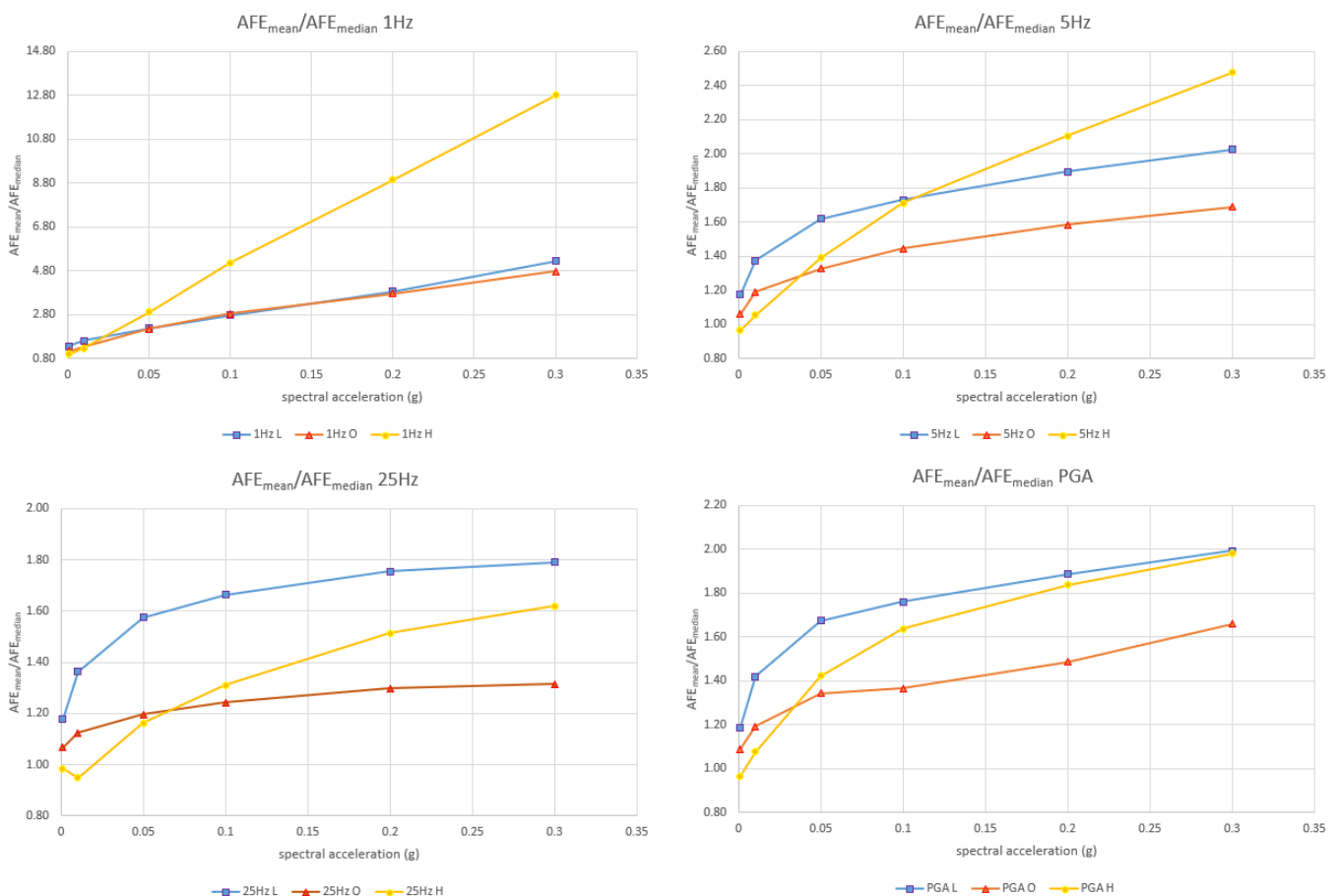


Figure 10. Ratio of AFE_{mean} and AFE_{median} at the Loviisa (L), Olkiluoto (O) and Hanhikivi (H), sites for spectral accelerations 0.001g, 0.01 g, 0.05 g, 0.1 g, 0.2 g, and 0.3 g and frequencies 1Hz, 5Hz, 25Hz, and PGA.



Table 5. AFE_{mean}/AFE_{median} ratio for spectral accelerations 0.001 g, 0.01 g, 0.05 g, 0.1 g, 0.2 g, and 0.3 g and frequencies 1Hz, 5Hz, 25Hz, and PGA for Hanhikivi (H), Loviisa (L) and Olkiluoto (O).

	0.001g	0.01g	0.05g	0.1g	0.2g	0.3g
1Hz L	1.36	1.61	2.19	2.79	3.87	5.24
5Hz L	1.18	1.38	1.62	1.73	1.90	2.02
25Hz L	1.18	1.36	1.57	1.67	1.76	1.79
PGA L	1.19	1.42	1.67	1.76	1.89	1.99
1Hz O	1.15	1.33	2.15	2.85	3.76	4.79
5Hz O	1.06	1.19	1.33	1.45	1.58	1.69
25Hz O	1.07	1.12	1.20	1.24	1.30	1.31
PGA O	1.09	1.19	1.34	1.37	1.49	1.66
1Hz H	1.01	1.28	2.93	5.17	8.96	12.81
5Hz H	0.97	1.06	1.39	1.71	2.10	2.48
25Hz H	0.98	0.95	1.16	1.31	1.51	1.62
PGA H	0.97	1.08	1.42	1.64	1.84	1.98

Finally, we present the AFEs that would give the same **mean** hazard values as the currently used **median** AFE 10^{-5} and 10^{-7} targets for DBE and DEC C (Figure 11). Since mean hazard always exceeds median, it is expected that the “mean-equivalent” AFEs are larger than 10^{-5} and 10^{-7} . We calculated the AFE for hypothetical “mean-equivalent” and “84 percentile-equivalent” hazard definition.

It can be noted that for DBE mean equivalent, AFE would be above 10^{-5} in the range of $2 \cdot 10^{-5}$ in most cases. However, the results are strongly dependent on the site and spectral frequency. The mean and median values are the closest for Olkiluoto and the highest for Hanhikivi. For Hanhikivi they are also more strongly frequency dependent. For 84th percentile equivalent DBE, AFE would be even higher in the range of $3 \cdot 10^{-5}$ for Hanhikivi and Loviisa and $2 \cdot 10^{-5}$ for Olkiluoto. For the DEC C earthquake, the change would mean an increase of the AFE from 10^{-7} to the range of $2 \cdot 10^{-7}$ in most cases. The precise target thresholds are given in Table 6.

Table 6. Target AFE for the three sites, if changing the hazard from mean to median and preserving the same hazard level.

	“Mean equivalent” AFE for	
	Design basis earthquake (DBE)	Design extension earthquake (DEC C)
Loviisa	1.62E-05	2.39E-07
Olkiluoto	1.27E-05	1.78E-07
Hanhikivi	1.57E-05	2.19E-07

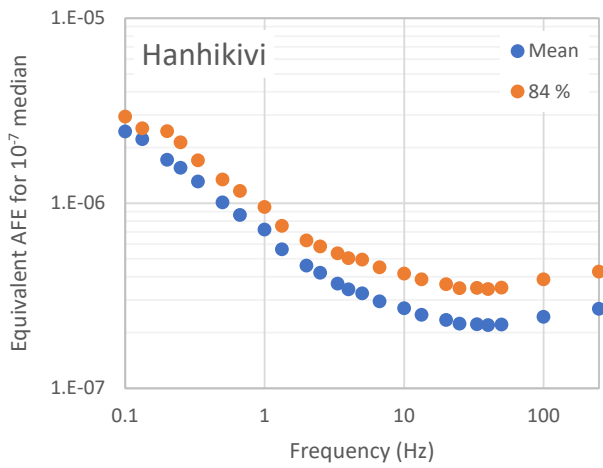
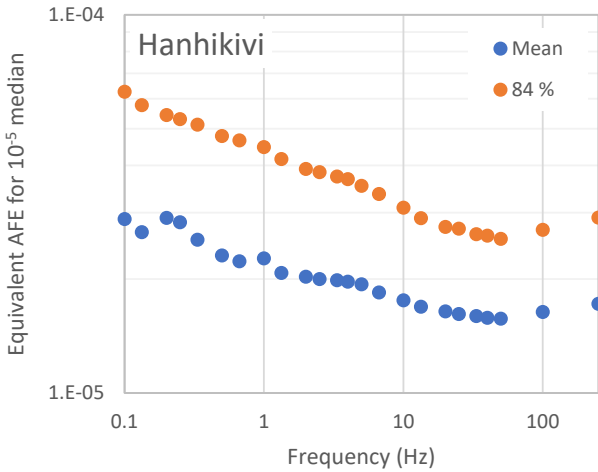
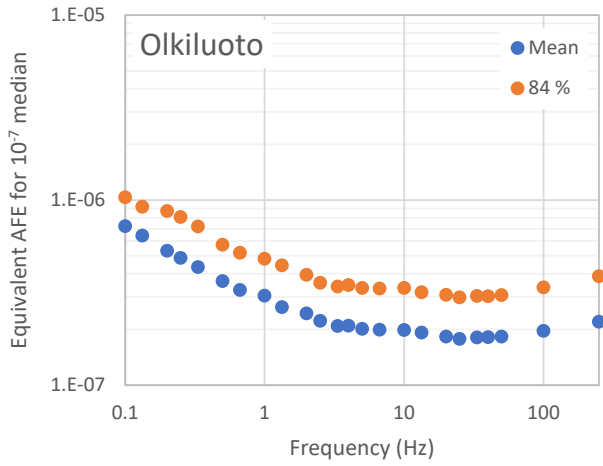
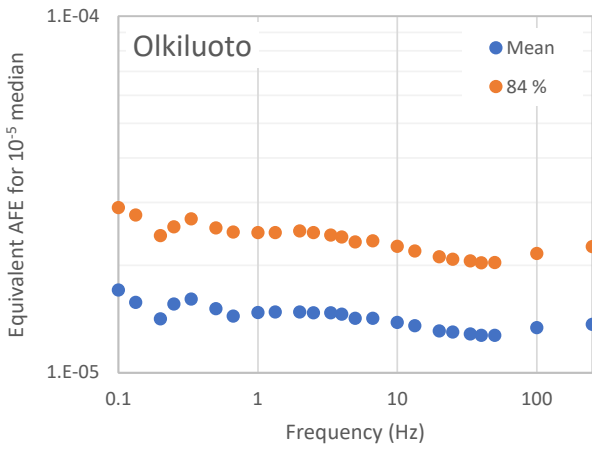
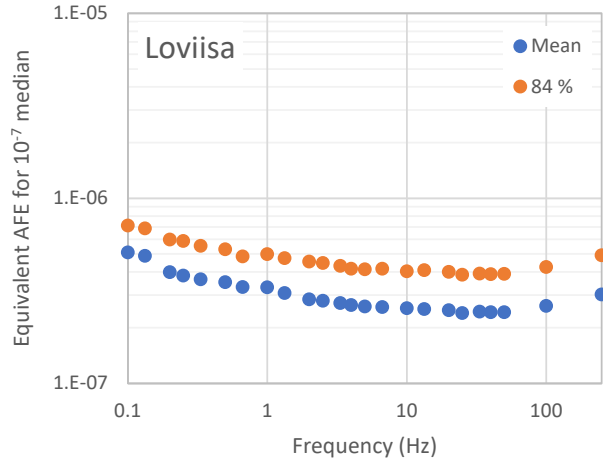
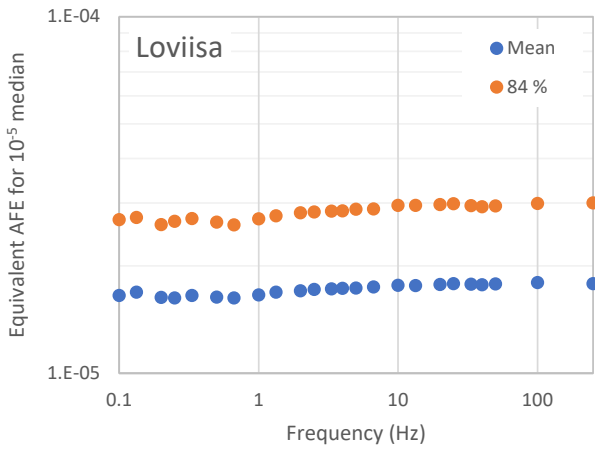


Figure 11. Target AFE for maintaining the current hazard level for DBE, equivalent to median AFE 10^{-5} and median AFE 10^{-7} in the case of a hypothetical change to mean or 84th percentile hazard.

7. Discussion and conclusions

The probability of an earthquake occurrence that generates ground motions beyond those of DBE at NPP sites is generally recognized to be small. This also applies to Finland, where an **M7** earthquake was evaluated as a very low-probability event (Koskinen 2013). There is nevertheless a regulatory need to evaluate ground motions beyond those of DBEs to guarantee that they would not lead to major failures in the performance of NPPs (so-called cliff-edge effects). There are also other reasons for carrying out similar evaluations, such as potentially inadequate seismic design due to the vintage of an NPP, or an increase in how seismic hazards are perceived at the target site (e.g. Johnson et al. 2017). In particular, perception of seismic hazards is often updated as new experience is obtained from real earthquakes. In 2004–2011, a cluster of megathrust earthquakes occurred on Earth after an intermission of 40 years and had a major impact on how seismic and tsunami hazards are perceived over the Indian Ocean and in the vicinity of Japan (e.g. Koyama et al. 2012). In addition to the epistemic uncertainty at the upper magnitude range at plate boundaries and continental interiors alike, the high variability of ground motions even from moderate earthquakes may warrant reconsiderations of seismic hazards (cf. Introduction).

There is currently no serious alternative for PSHA (section 2) in sight, despite some criticism (e.g. Mulargia et al. 2017). Gerstenberger et al. (2020) consider the future direction to be a better quantification of the uncertainties in knowledge of earthquake processes (which may have been spurred by the criticism). Quantification and reduction in the reducible uncertainties of seismic hazards are emphasized. Ideally, new extensive datasets allow the validation of individual hazard model inputs (e.g. Daxer et al. 2022), but the limited time spans of available seismicity records remain a major obstacle here. In the Fennoscandian Shield, paleoseismology is associated with the end-glacial stress field and is not considered in NPP-related PSHAs.

The current review supports the notion that mean hazards are prevalently targeted for engineering design. The mean hazard is in line with probabilistic risk analysis (section 3) and is the choice for NPPs in several European OECD member countries (section 5). That the mean represents a composite of all hazards (section 4) is relevant to Finland as well, since low-probability earthquake scenarios are the key elements in PSHA for NPPs. For example, if a future earthquake scenario, say a magnitude **M7.0** event occurring in Finland, is considered plausible but extremely rare, it is associated with a low weight in the logic tree. A median hazard would entirely erase the scenario, while the mean hazard would still keep it, notwithstanding some debate among the experts about the exact value of the weight. At very low AFEs, the mean hazard increases over many fractiles. The practice is often to report a number of fractiles and the mean hazard, whether the focus is on hazard mapping for general building codes (Danciu et al. 2021) or for critical infrastructure such as NPPs (Abrahamson et al. 2004). The mean is always larger than the median, as long as peak-ground-motion parameters follow the lognormal distribution, so selection of the hazard curve to read for a ground-motion value affects the adoption of the corresponding AFE. For deterministic design, the mean, median or other fractiles can be used and are used in existing nuclear practice.

Current analyses based on the SENSEI set of calculations show a variety of hazard levels at the three sites for various frequencies. For the DBE mean equivalent, the AFE would be above the range of $2 \cdot 10^{-5}$ in most cases. However, the results must be evaluated separately for each site and spectral frequency. The mean and median values are closest for Olkiluoto and highest for Hanhikivi. For Hanhikivi, they are also more strongly frequency-dependent. For 84th percentile equivalent DBE, AFE would be even higher in the range of AFE $3 \cdot 10^{-5}$ for Hanhikivi and Loviisa and AFE $2 \cdot 10^{-5}$ for Olkiluoto. For a DEC C earthquake, the change would be to increase the AFE from 10^{-7} to the range of $2 \cdot 10^{-7}$ in most cases.

We recommend that PSHA outputs should be reported for the mean, median, and the 5th, 16th, 84th, and 95th fractile hazard curves to allow future decision-makers to consider the uncertainties in an appropriate manner. Such reporting also gives stable grounds for comparison of new PSHA models with previous ones. Comparison of models should not only use solitary ground-motion design values, although they are clearly the output of major interest.



Acknowledgement

This work was financially supported by the Finnish Nuclear Power Plant Safety Research Programme 2019–2022 (SAFIR2022).

References

Publications

- Abrahamson, N.A., Bommer, J.J., 2005. Probability and uncertainty in seismic hazard analysis. *Earthquake Spectra* 21:603–607
- Abrahamson, N.A., Coppersmith, K.J., Koller, M., Roth, P., Sprecher, C., Toro, G.R., Youngs, R., 2004. Probabilistic seismic hazard analysis for Swiss nuclear power plant sites (PEGASOS Project), Final Report, Vol. 1 (text). Retrieved from <https://www.swissnuclear.ch/upload/cms/user/PEGASOSProjectReportVolume1-new.pdf>
- Basham, P., Giardini, D., 1993. Technical guidelines for global seismic hazard assessment. *Ann. Geofis.* 36:15–24. <https://doi.org/10.4401/ag-4257>
- Bazzurro, P., Cornell, C.A., 1999. Disaggregation of seismic hazard. *Bull. Seismol. Soc. Am.* 89:501–520
- Bommer, J. J., 2012. Challenges of building logic trees for probabilistic seismic hazard analysis. *Earthquake Spectra* 28:1723–1735. <https://doi.org/10.1193/1.4000079>
- Bommer, J. J., Scherbaum, F., Bungum, H., Cotton, F., Sabetta, F., Abrahamson, N.A., 2005. On the use of logic trees for ground-motion prediction equations in seismic-hazard analysis. *Bull. Seismol. Soc. Am.* 95:377–389. <https://doi.org/10.1785/0120040073>
- Bommer, J.J., Scherbaum, F., 2008. The use and misuse of logic trees in probabilistic seismic hazard analysis. *Earthquake Spectra* 24:997–1009. <https://doi.org/10.1193/1.2977755>
- Budnitz, R. J., Apostolakis, G., Boore, D. M., Cluff, L. S., Coppersmith, K. J., Cornell, C. A., Morris, P. A., 1997a. Recommendations for Probabilistic Seismic Hazard Analysis: Guidance on uncertainty and use of experts. NUREG/CR-6372 UCRL- ID – 122160, vol. 1
- Budnitz, R. J., Apostolakis, G., Boore, D. M., Cluff, L. S., Coppersmith, K. J., Cornell, C. A., Morris, P. A., 1997b. Recommendations for Probabilistic Seismic Hazard Analysis: Guidance on uncertainty and use of experts. Appendices. NUREG/CR-6372 UCRL- ID – 122160, vol. 2
- Cornell, C. A., 1968. Engineering seismic risk analysis. *Bull. Seismol. Soc. Am.* 58:1583–1606. Erratum 59:1733
- Cornell, C.A., Krawinkler, H., 2000. Progress and challenges in seismic performance assessment. *PEER Center News*, 3, 1-3
- Danciu, L., Nandan, S., Reyes, C., Basili, R., Weatherill, G., Beauval, C., Rovida, A., Vilanova, S., Sesetyan, K., Bard P.-Y., Cotton, F., Wiemer, S., Giardini, D., 2021. The 2020 update of the European Seismic Hazard Model: Model overview. EFER Technical Report 001, v1.0.0, [doi:10.12686/a15](https://doi.org/10.12686/a15)
- Daxer, C., Huang, J.-J.S., Weginger, S., Hilbe, M., Strasser, M., Moernaut, J., 2022. Validation of seismic hazard curves using a calibrated 14 ka lacustrine record in the Eastern Alps, Austria. *Sci. Rep.* 12:19943. <https://doi.org/10.1038/s41598-022-24487-w>
- Deierlein, G., Krawinkler, H., Cornell, C., 2003. A framework for performance-based earthquake engineering. Pacific Conference on Earthquake EngineeringAt: Christchurch, New Zealand, 2003
- Deierlein G, Moehle J. 2004. A Framework for performance-based earthquake engineering. Proceedings of an International Workshop on Performance-Based Seismic Design – Concepts and Implementation, Bled, Slovenia.



- Fülöp, L., Mäntyniemi, P., Malm, M., Toro, G., Crespo, M.J., Schmitt, T., Burck, S., Välikangas, P., 2022. Probabilistic seismic hazard analysis in low-seismicity regions: An investigation of sensitivity with a focus on Finland. *Nat. Hazards*, <https://doi.org/10.1007/s11069-022-05666-4>
- Geller, R.J., 2011. Shake-up time for Japanese seismology. *Nature* 472:407–409
- Gerstenberger, M. C., Marzocchi, W., Allen, T., Pagani, M., Adams, J., Danciu, L. et al., 2021. Probabilistic seismic hazard analysis at regional and national scales: State of the art and future challenges. *Rev. Geophys.* 58: e2019RG000653. doi:10.1029/2019RG000653
- Giardini, D., Basham, P., 1993. The Global Seismic Hazard Assessment Program (GSHAP). *Ann. Geofis.* 36:3–13. <https://doi.org/10.4401/ag-4256>
- Goulet, C.A., Bozorgnia, Y., Abrahamson, N., Kuehn, N., Al Atik, L., Youngs, R., Graves, R., Atkinson, G. (2018) Central and Eastern North America ground-motion characterization NGA-East. Final Report (No. PEER 2018/08). Pacific Earthquake Engineering Research Center, California, Berkeley
- Goulet, C. A., Bozorgnia, Y., Kuehn, N., Al Atik, L., Youngs, R. R., Graves, R. W., Atkinson, G. M., 2021. NGA-East ground-motion characterization model Part I: Summary of products and model development. *Earthquake Spectra* 37(1_suppl):1231–1282
- Hanks, T. C., Beroza, G. C., Toda, S., 2012. Have recent earthquakes exposed flaws in or misunderstandings of probabilistic seismic hazard analysis? *Seismol. Res. Lett.* 83:759–764. <https://doi.org/10.1785/0220120043>
- Hauksson, E., Jones, L. M., Hutton, K., Eberhart-Phillips, D., 1993. The 1992 Landers earthquake sequence: Seismological observations. *J. Geophys. Res.* 98:19,835–19,858
- Huang, Y.-N., Whittaker, A. S., Luco, N., 2011. A probabilistic seismic risk assessment procedure for nuclear power plants: (I) Methodology. *Nucl. Eng. Des.* 241:3996–4003. <https://doi.org/10.1016/j.nucengdes.2011.06.051>
- IAEA, 2011. Earthquake preparedness and response for nuclear power plants. International Atomic Energy Agency IAEA Safety Reports Series No. 66
- IAEA, 2012. Safety of Nuclear Power Plants: Design. International Atomic Energy Agency IAEA Specific Safety Requirements Series No. SSR-2/1, Vienna, Austria
- IAEA, 2016. Safety of Nuclear Power Plants: Design. International Atomic Energy Agency IAEA Specific Safety Requirements Series No. SSR-2/1 (Rev 1), Vienna, Austria
- Johnson, J. J., Gürpınar, A., Campbell, R. D., Kammerer, A., Rivera-Lugo, R., Stovall, S., 2017. Seismic design standards and calculational methods in the United States and Japan. United States Nuclear Regulatory Commission, Report NUREG/CR-7230
- Koskinen, P., 2013. Orientation of faults and their potential for reactivation in the present stress field in Finland. MSc thesis, Department of Physics, University of Helsinki, Finland, 64 pp. permalink <http://urn.fi/URN:NBN:fi-fe2017112251755>
- Koyama, J., Yoshizawa, K., Yomogida, K., Tsuzuki, M., 2012. Variability of megathrust earthquakes in the world revealed by the 2011 Tohoku-oki earthquake. *Earth Planets Space* 64:1189–1198. <https://doi.org/10.5047/eps.2012.04.011>
- Krawinkler H, Miranda E., 2004, Performance-based earthquake engineering. *Earthquake Engineering: from engineering seismology to performance-based engineering*, Chapter 9. CRC Press: Danvers, MA, USA
- Kulkarni, R.B., Youngs, R.R., Coppersmith, K.J., 1984. Assessment of confidence intervals for results of seismic hazard analysis. In: *Proceedings, Eighth World Conference on Earthquake Engineering*, vol. 1, San Francisco, pp. 263–270
- Mäntyniemi, P., Sørensen, M.B., Tatevossian, R.E., 2021a. Testing the Environmental Seismic Intensity scale on data derived from the earthquakes of 1626, 1759, 1819, and 1904 in Fennoscandia, northern Europe. *Geosciences* 11, 14. <https://doi.org/10.3390/geosciences11010014>



- Mäntyniemi, P., Malm, M., Burck, S., Okko, O., Välikangas, P., Fülöp, L., 2021b. Sensitivity of seismic hazard analysis in Finland: Overview of the SENSEI project. *ATS Ydintekniikka* 50(2):19–23
- Marzocchi, W., Jordan, T. H., 2014. Testing for ontological errors in probabilistic forecasting models of natural systems. *Proceedings of the National Academy of Sciences* 111(33):11973–11978, <https://doi.org/10.1073/pnas.1410183111>.
- Marzocchi, W., Taroni, M., Selva, J., 2015. Accounting for epistemic uncertainty in PSHA: logic tree and ensemble modeling. *Bull. Seismol. Soc. Am.* 105:2151–2159. <https://doi.org/10.1785/0120140131>
- McGuire, R.K., 1977. Effects of uncertainty on estimates of seismic hazard for the east coast of the United States. *Bull. Seismol. Soc. Am.* 67:827–848
- McGuire, R.K., 1993. Computations of seismic hazard. *Ann. Geofis.* 36:181–200. <https://doi.org/10.4401/ag-4263>
- McGuire, R.K., Cornell, C.A., Toro, G.R., 2005. The case for using mean seismic hazard. *Earthquake Spectra* 21:879–886. <https://doi.org/10.1193/1.1985447>
- Minson, S. E., Baltay, A. S., Cochran, E. S., McBride, S. K., Milner, K. R., 2020. Shaking is almost always a surprise: the earthquakes that produce significant ground motion. *Seismol. Res. Lett.* 92:460–468. <https://doi.org/10.1785/0220200165>
- Mulargia, F., Stark, P.B., Geller, R.J., 2017. Why is probabilistic seismic hazard analysis (PSHA) still used? *Phys. Earth Planet. In.* 264:63–75. <https://doi.org/10.1016/j.pepi.2016.12.002>
- Musson, R.M.W., 2005. Against fractiles. *Earthquake Spectra* 21:887–891
- Nicholson, C., Roeloffs, E., Wesson, R.L., 1988. The northeastern Ohio earthquake of 31 January 1986: Was it induced? *Bull. Seismol. Soc. Am.* 78:188–217
- Nöggerath, J., Geller, R.J., Gusiakov, V.K., 2012. Fukushima: the myth of safety, the reality of geoscience. *Bull. Atomic Sci.* 67:37–46
- Norio, O., Ye, T., Kajitani, Y., Shi, P., Tatano, H., 2011. The 2011 Eastern Japan great earthquake disaster: overview and comments. *Int. J. Disaster Risk Sci.* 2:34–42. <https://doi.org/10.1007/s13753-011-0004-9>
- OECD, 2019. Comparison of probabilistic seismic hazard analysis of nuclear power plants in areas with different levels of seismic activity. Report NEA/CSNI/R(2019)1, Organization for Economic Co-operation and Development Nuclear Energy Agency (NEA), Paris
- Okko, O., Fülöp, L., Sandberg, J., Välikangas, P., 2019. Comparison of probabilistic seismic hazard studies within the oecd countries, Proceedings of the Symposium on the Application of Geophysics to Engineering and Environmental Problems, SAGEEP 2019, Portland, United States
- Scherbaum, F., Kuehn, N. M., 2011. Logic tree branch weights and probabilities: Summing up to one is not enough. *Earthquake Spectra* 27:1237–1251
- Stein, S., Geller, R., Liu, M., 2011. Bad assumptions or bad luck: Why earthquake hazard maps need objective testing. *Seismol. Res. Lett.* 82:623–626
- Stepp, J.C., Wong, I., Whitney, J., Quittmeyer, R., Abrahamson, N., Toro, G., Youngs, R., Coppersmith, K., Savy, J., Sullivan, T. & Yucca Mountain PSHA project members, 2001. Probabilistic seismic hazard analysis for ground motions and fault displacements at Yucca Mountain, Nevada. *Earthquake Spectra* 17:113–151
- STUK, 2019. Guide YVL B.7 Provisions for internal and external hazards at a nuclear facility. Radiation and Nuclear Safety Authority. Retrieved from <https://www.stuklex.fi/en/YVLB.7-memo.pdf>
- Uski, M., Lund, B., Korja, A., 2015. Observed depth of seismicity. In Korja, A., Kosonen, E. (Eds.), *Seismotectonic framework and seismic source area models in Fennoscandia, Northern Europe*. Report S-63, Institute of Seismology, University of Helsinki, 129–131.



Wong, I. G., 2014. How big, how bad, how often: are extreme events accounted for in modern seismic hazard analyses? *Nat. Hazards* 72:1299–1309. <https://doi.org/10.1007/s11069-013-0598-x>

Youngs, R. R., Goulet, C. A., Bozorgnia, Y., Kuehn, N., Al Atik, L., Graves, R. W., Atkinson, G. M., 2021. NGA-East ground-motion characterization model Part II: Implementation and hazard implications. *Earthquake Spectra* 37(1_suppl):1283–1330

WENRA, 2020. Western European Nuclear Regulators Association Reactor Safety Reference Levels. Retrieved from https://www.wenra.eu/sites/default/files/publications/wenra_guidance_on_seismic_events_-_2020-06-01.pdf

Zareian, F., Krawinkler, H., 2012. Conceptual performance-based seismic design using building-level and story-level decision support system. *Earthquake Eng. Struct. Dynam.* 41:1439–1453. <https://doi.org/10.1002/eqe.2218>

Websites

WNO: <https://world-nuclear.org/information-library/safety-and-security/safety-of-plants/nuclear-power-plants-and-earthquakes.aspx>

(last accessed 30 September 2022)



Appendix 1

A list of seismotectonic hazards according to the Western European Nuclear Regulators Association (WENRA) 2020, p. 7–8

Ground-motion hazards and the potential for fault displacement

- Vibratory ground motion (ground shaking waves due to earthquakes propagated from both far and near field fault rupture processes), including long period waves and short period waves
- Near fault effects on long period ground motion with very short duration (0.5–5 s) (forward directivity and fling-step ground motion observed from velocity pulses recorded in time histories)
- Site effects. Free field vibratory ground motion amplification/deamplification due to: a) Variations in the site-specific shear-wave velocity profile from seismic bedrock (shear-wave velocity up to ≈ 3 km/s) to the surface b) Site topography c) Basin geologic structure
- Surface faulting from the main or secondary fault ruptures (“fault capability”; ground displacement or surface rupture at or near the site surface due to co-seismic movements at a fault)

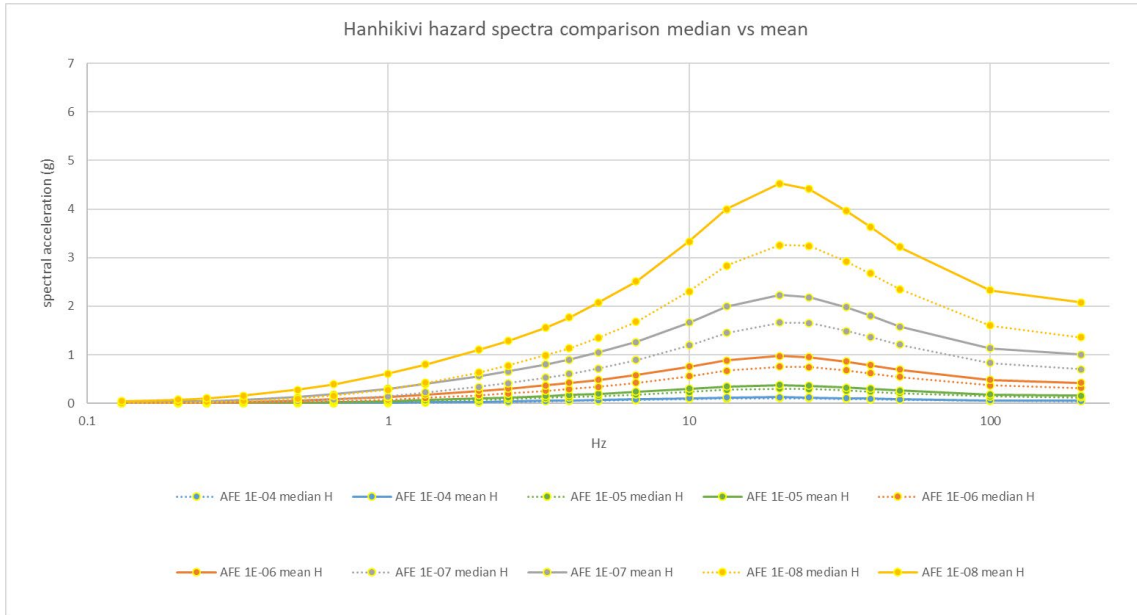
Hazard phenomena triggered by seismotectonic events

- Liquefaction (ground failure undermining the foundations and base courses of structures caused by water saturated sediments that are transformed into a substance that acts like a liquid during seismic shaking)
- Dynamic compaction (natural soil and human-made fillings: settlement induced by seismic shaking)
- Ground collapse (in areas of suberosion processes, e.g., by karstification)
- Earthquake-induced slope instability, debris or mud flow (mass movements of water-saturated sediments), and underwater landslides
- Flooding/drawdown by tsunami and seiche (a series of water waves caused by the displacement of a volume of a body of water, typically an ocean or large lake)
- Failure of dams or other water containment structures and flood protection systems
- External human-made hazards such as industrial and traffic accidents (e.g. chemical release, jet fire from a gas pipe line, external explosion)
- Loss of infrastructure, e.g. grid supplies
- Triggered internal events such as flooding, fire, or steam release

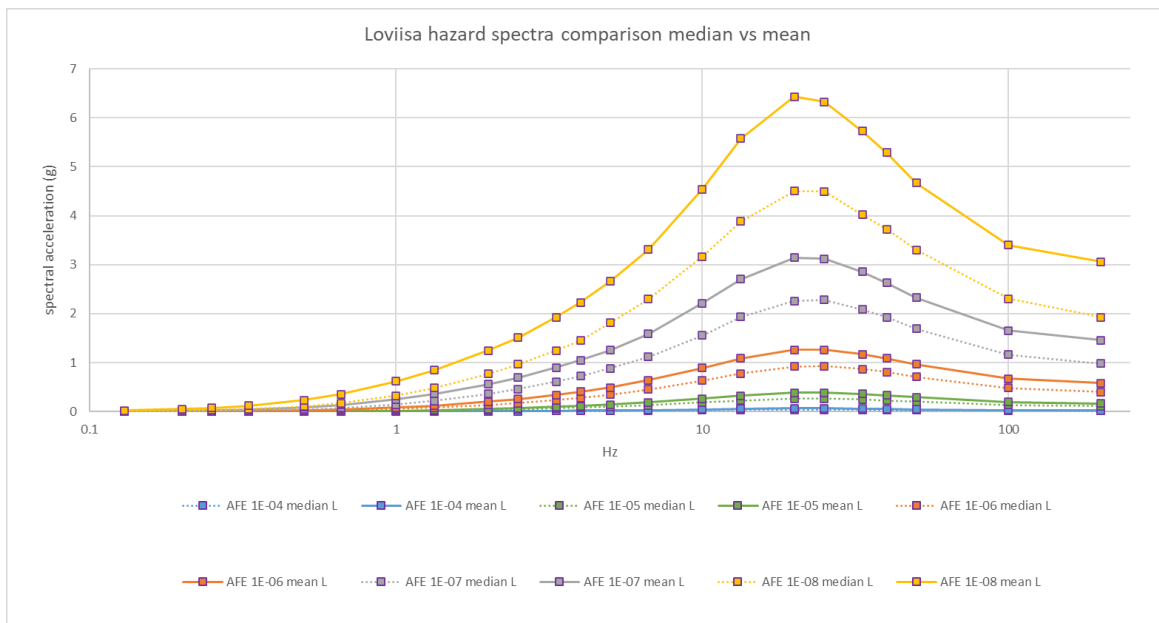


Appendix 2

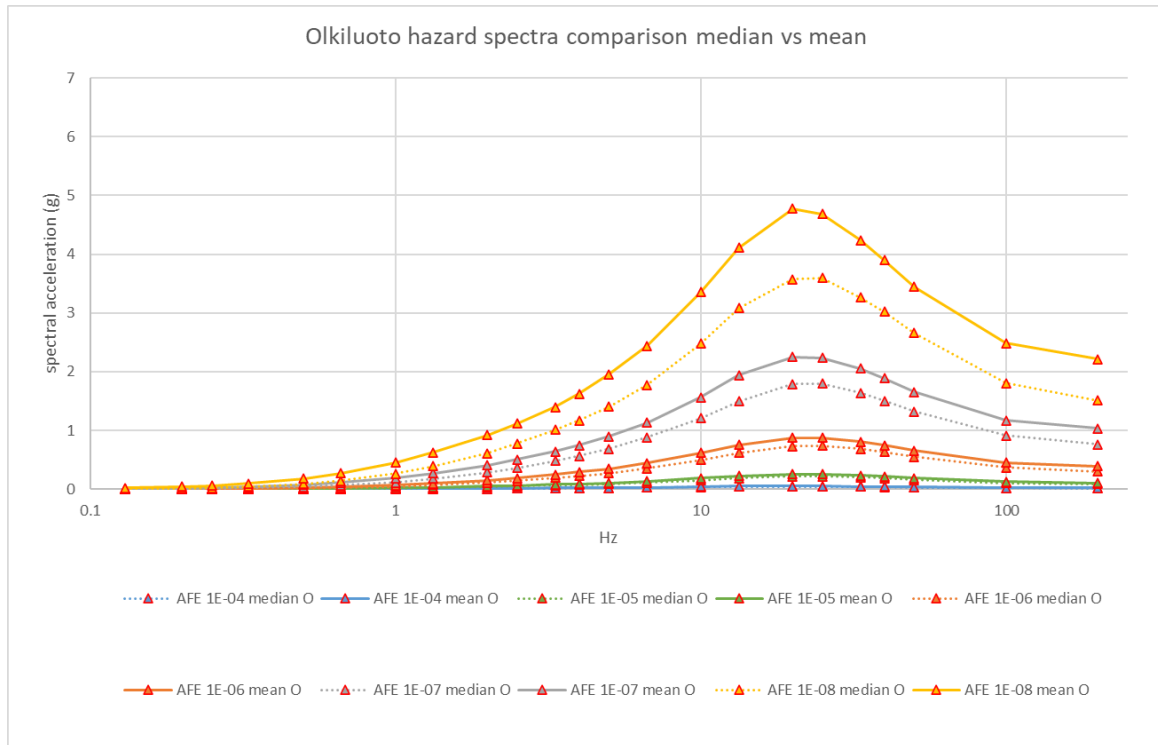
Additional figures based on the SENSEI hazard calculations.



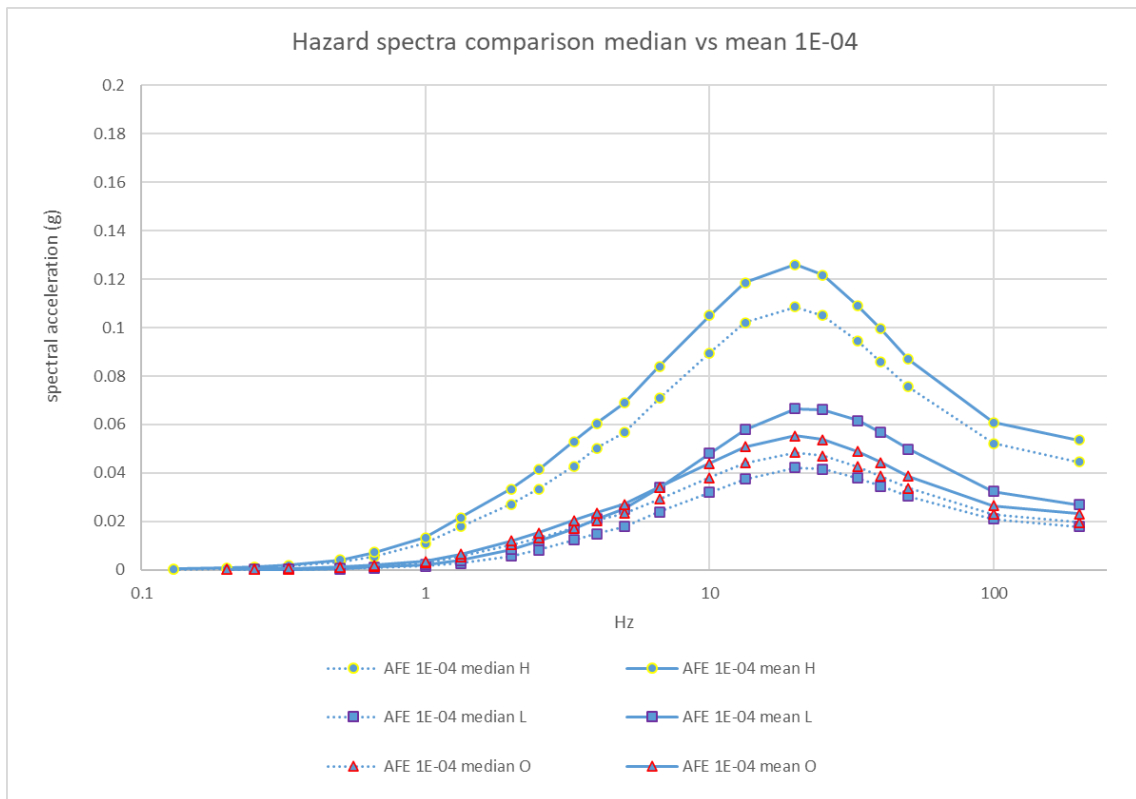
Median and mean hazard spectra for Hanhikivi (H) at AFE levels 10^{-4} to 10^{-8} . PGA is plotted at 200Hz.



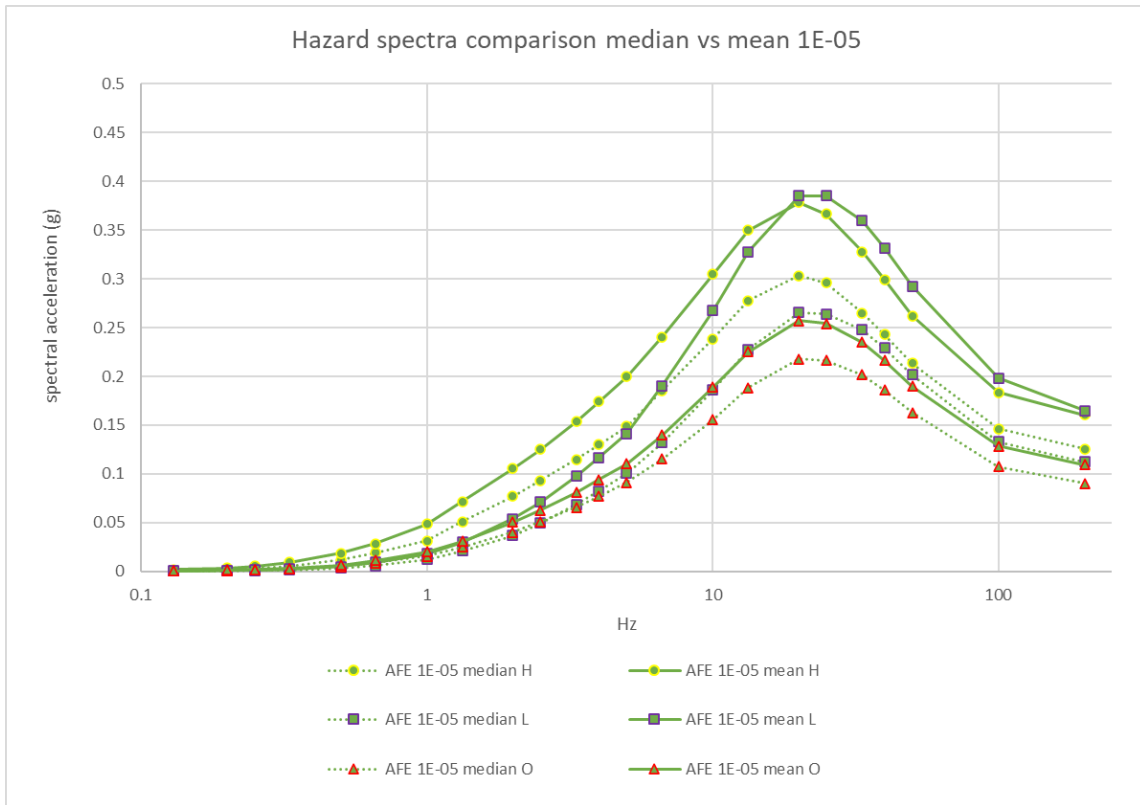
Median and mean hazard spectra for Loviisa (L) at AFE levels 10^{-4} to 10^{-8} . PGA is plotted at 200Hz.



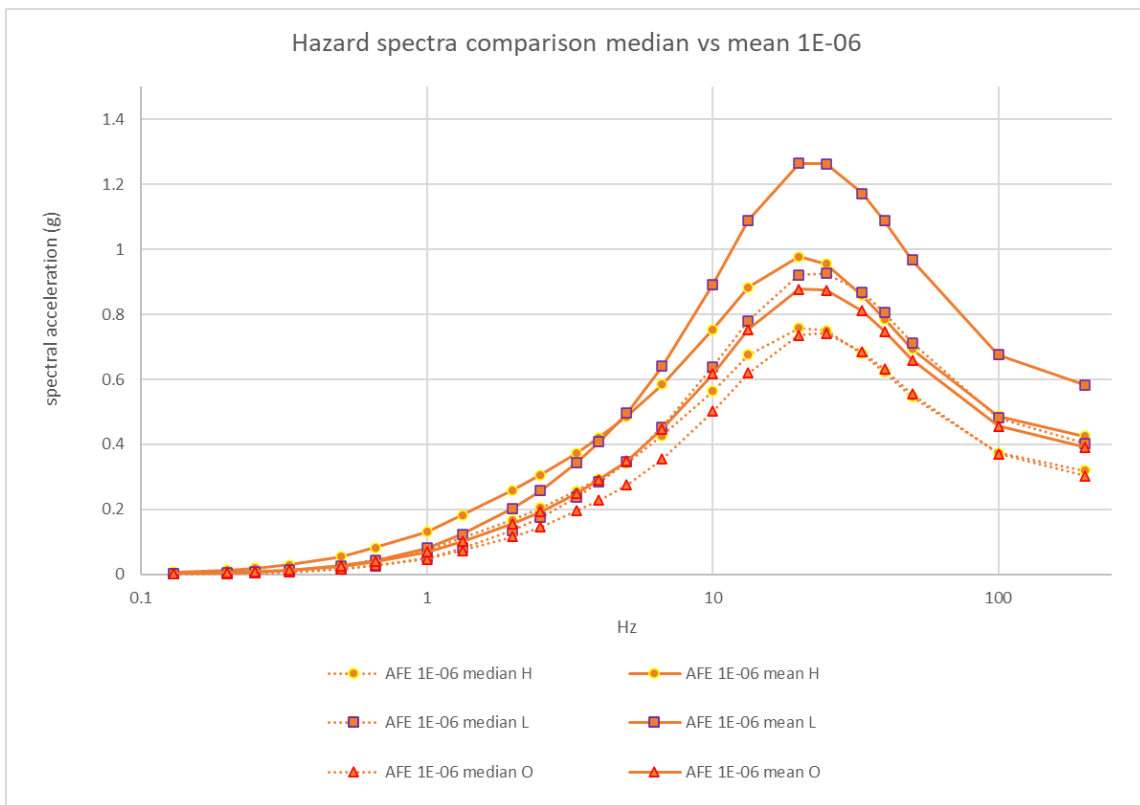
Median and mean hazard spectra for Olkiluoto (O) at AFE levels 10^{-4} to 10^{-8} . PGA is plotted at 200Hz.



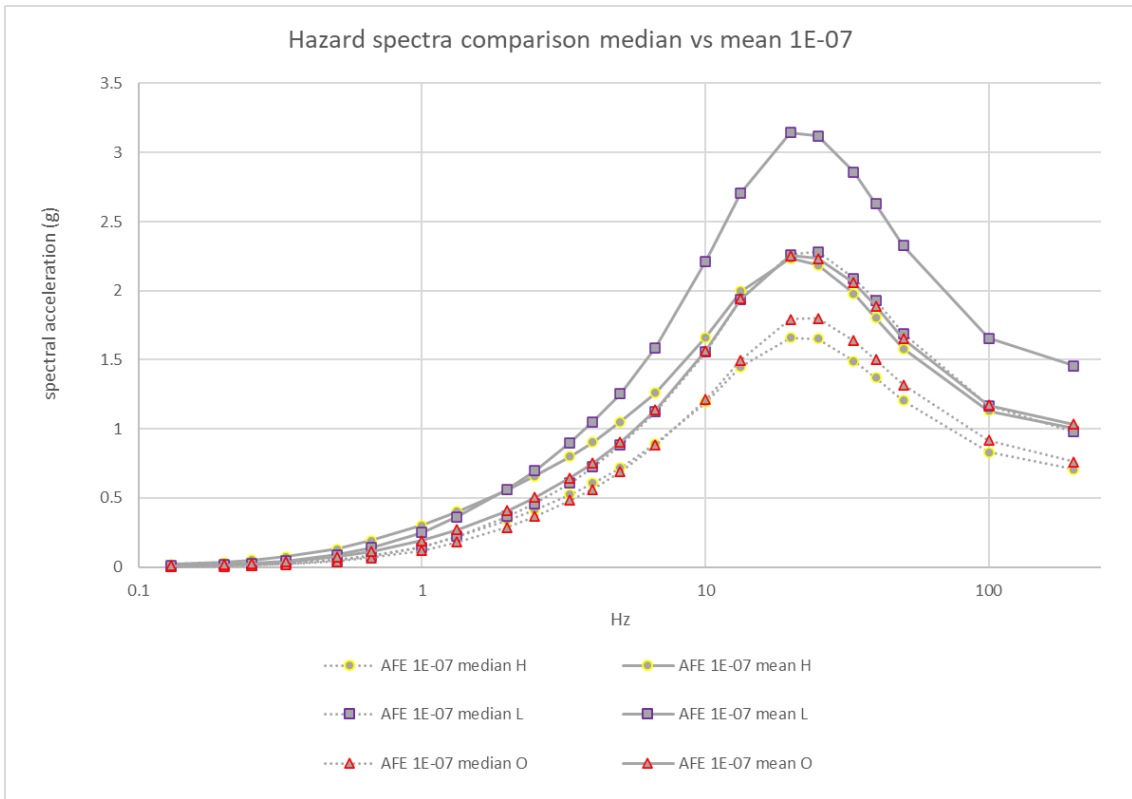
Median and mean hazard spectra comparison for Hanhikivi (H, yellow circle), Loviisa (L, purple square), and Olkiluoto (O, red triangle) at AFE level 10^{-4} . PGA is plotted at 200Hz.



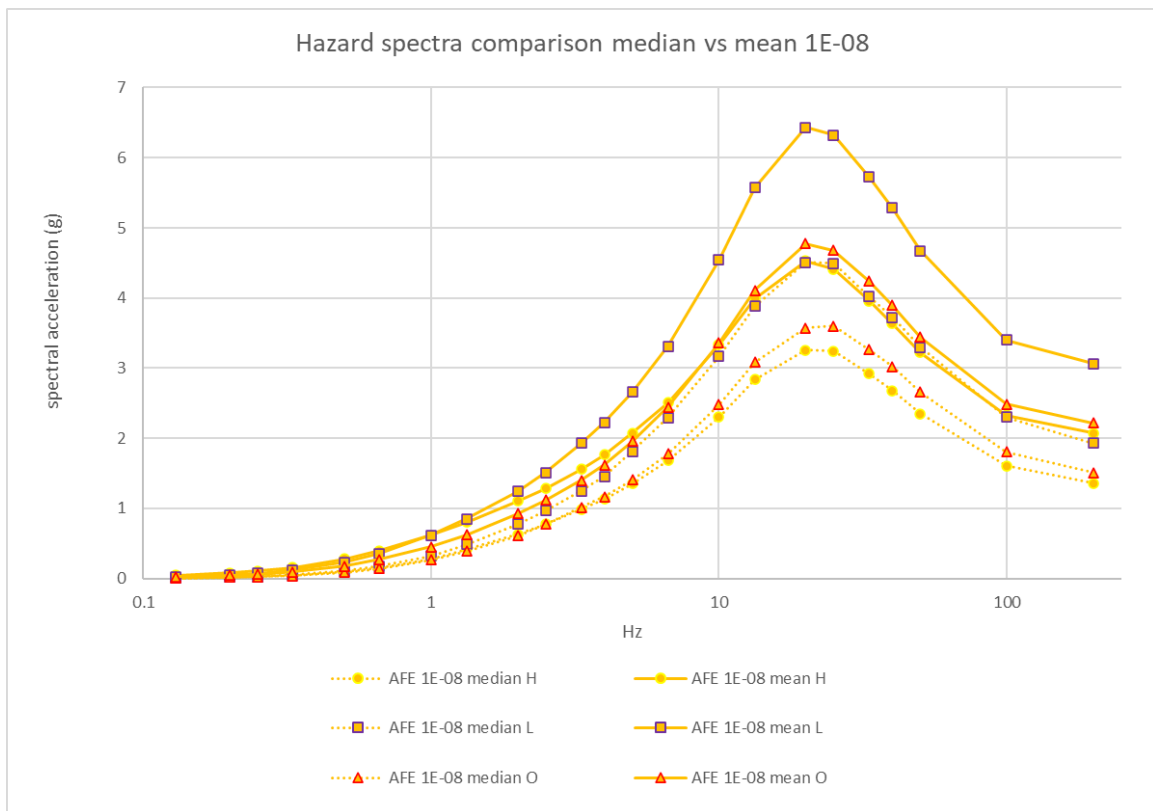
Median and mean hazard spectra comparison for Hanhikivi (H, yellow circle), Loviisa (L, purple square), and Olkiluoto (O, red triangle) at AFE level 10^{-5} . PGA is plotted at 200Hz.



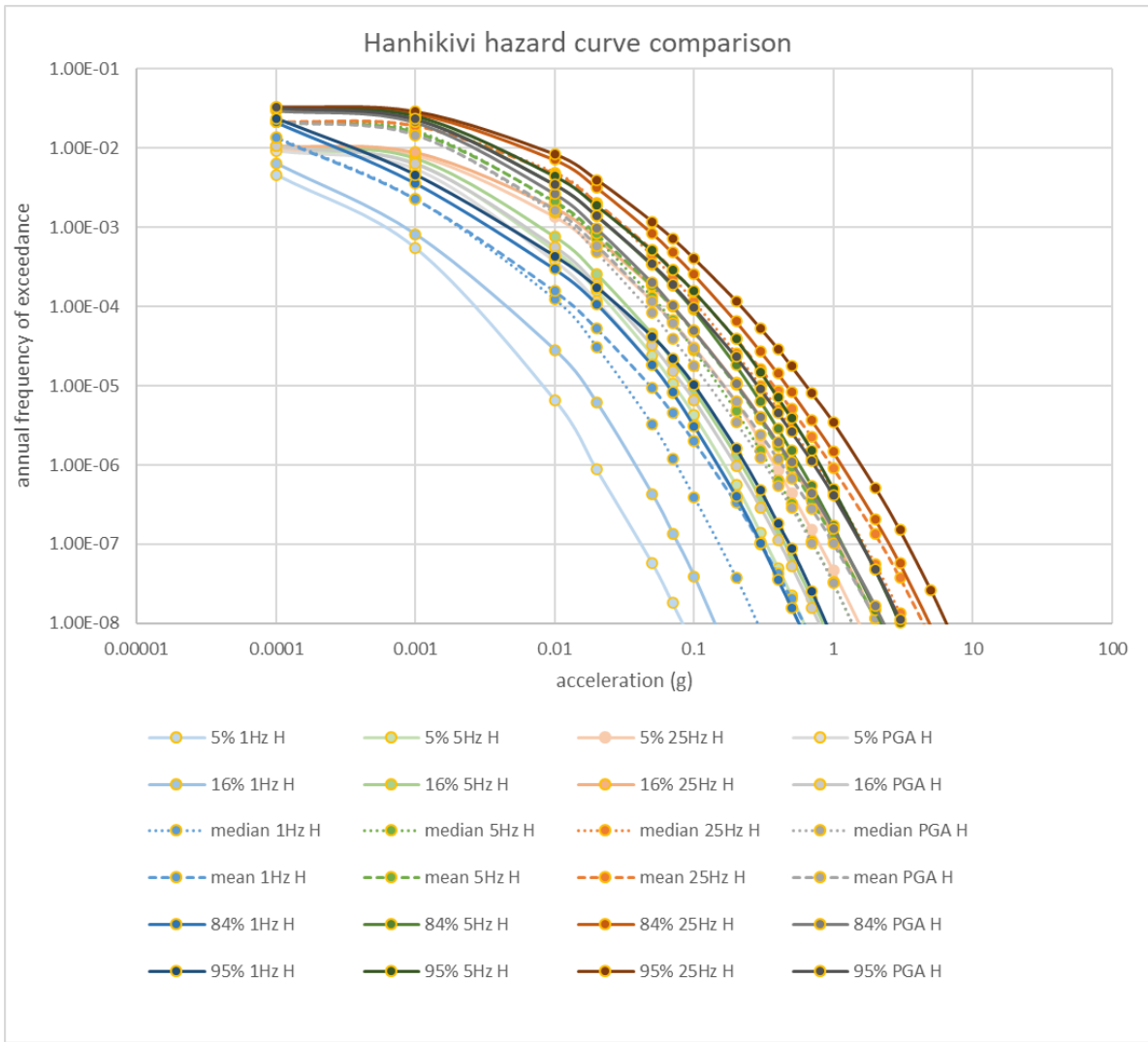
Median and mean hazard spectra comparison for Hanhikivi (H, yellow circle), Loviisa (L, purple square), and Olkiluoto (O, red triangle) at AFE level 10^{-6} . PGA is plotted at 200Hz.



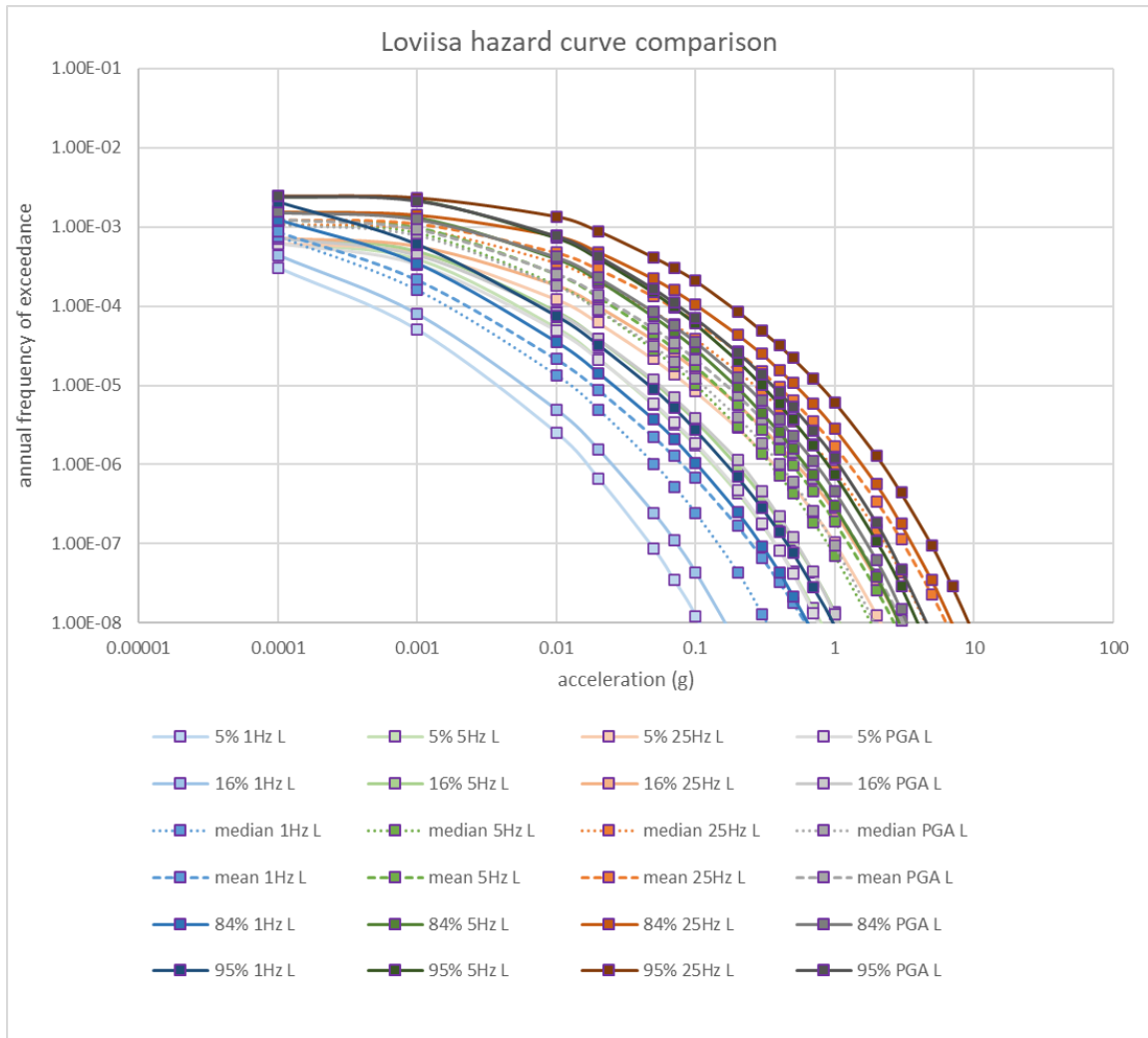
Median and mean hazard spectra comparison for Hanhikivi (H, yellow circle), Loviisa (L, purple square), and Olkiluoto (O, red triangle) at AFE level 10^{-7} . PGA is plotted at 200Hz.



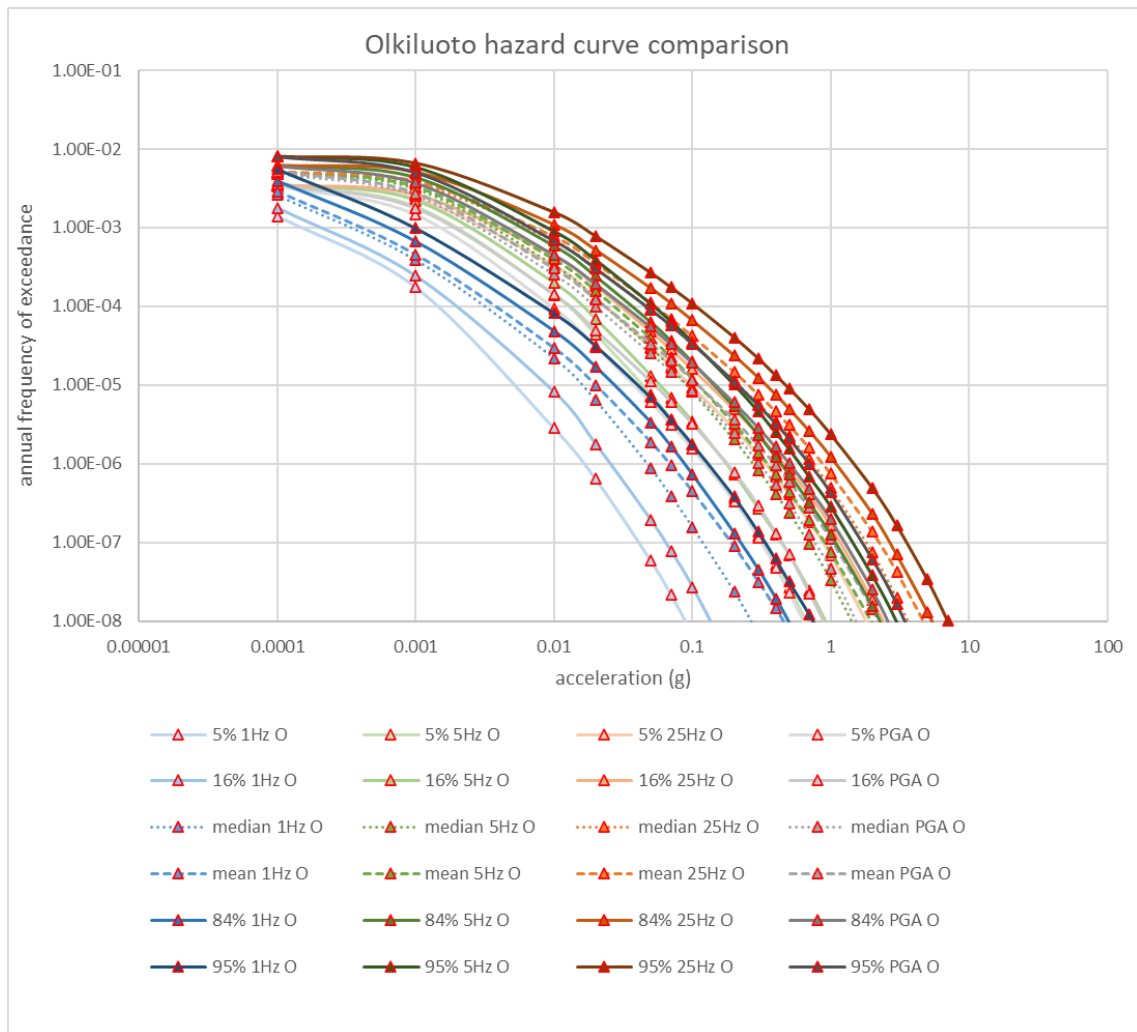
Median and mean hazard spectra comparison for Hanhikivi (H, yellow circle), Loviisa (L, purple square), and Olkiluoto (O, red triangle) at AFE level 10^{-8} . PGA is plotted at 200Hz.



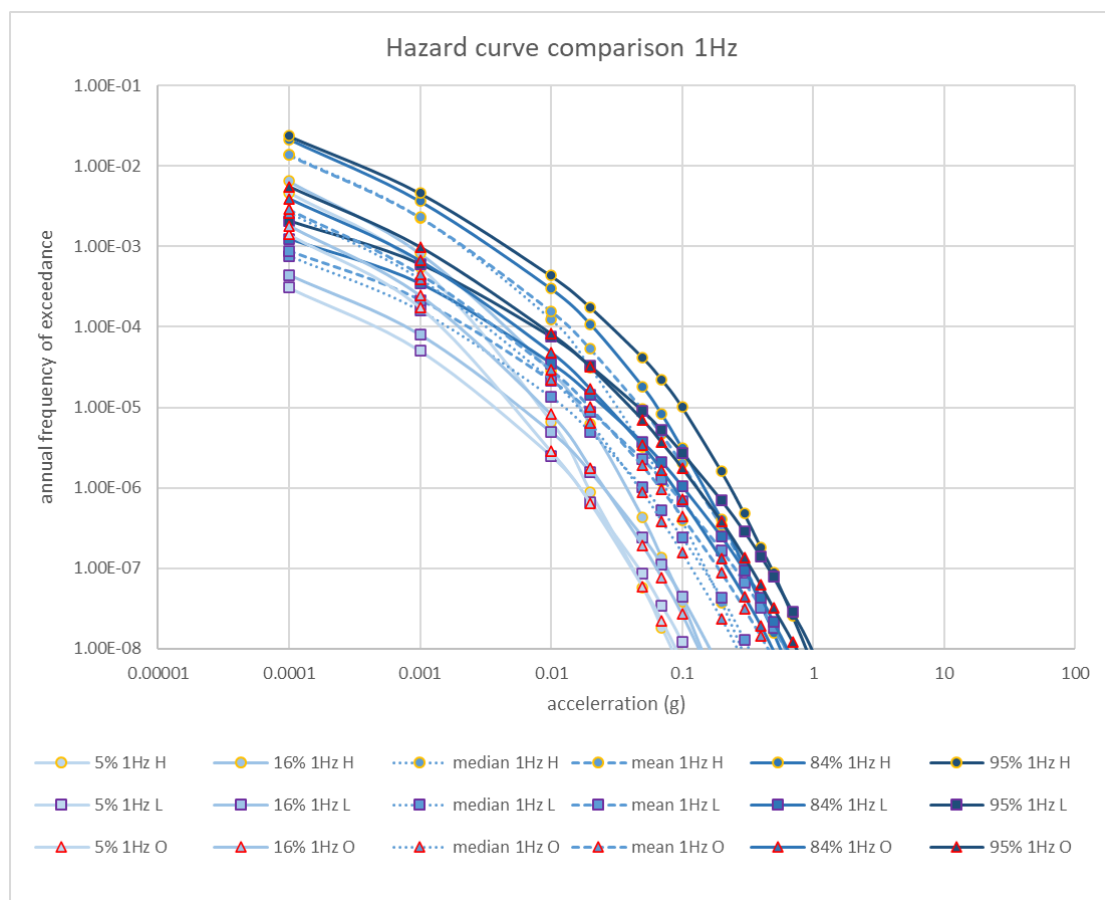
Hanhikivi hazard curves for 5%, 16%, median (50%), mean, 84%, and 95% percentiles for 1Hz, 5Hz, 25Hz, and PGA.



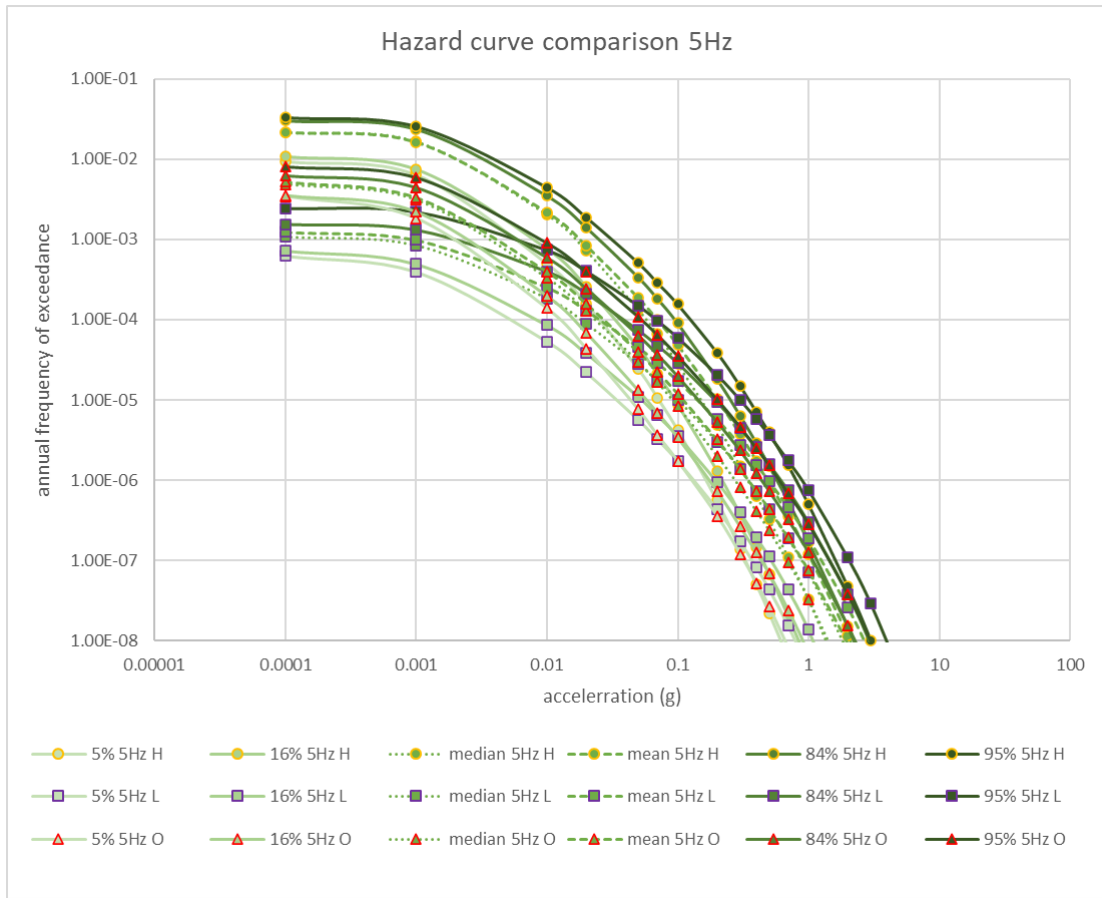
Loviisa hazard curves for 5%, 16%, median (50%), mean, 84%, and 95% percentiles for 1Hz, 5Hz, 25Hz, and PGA.



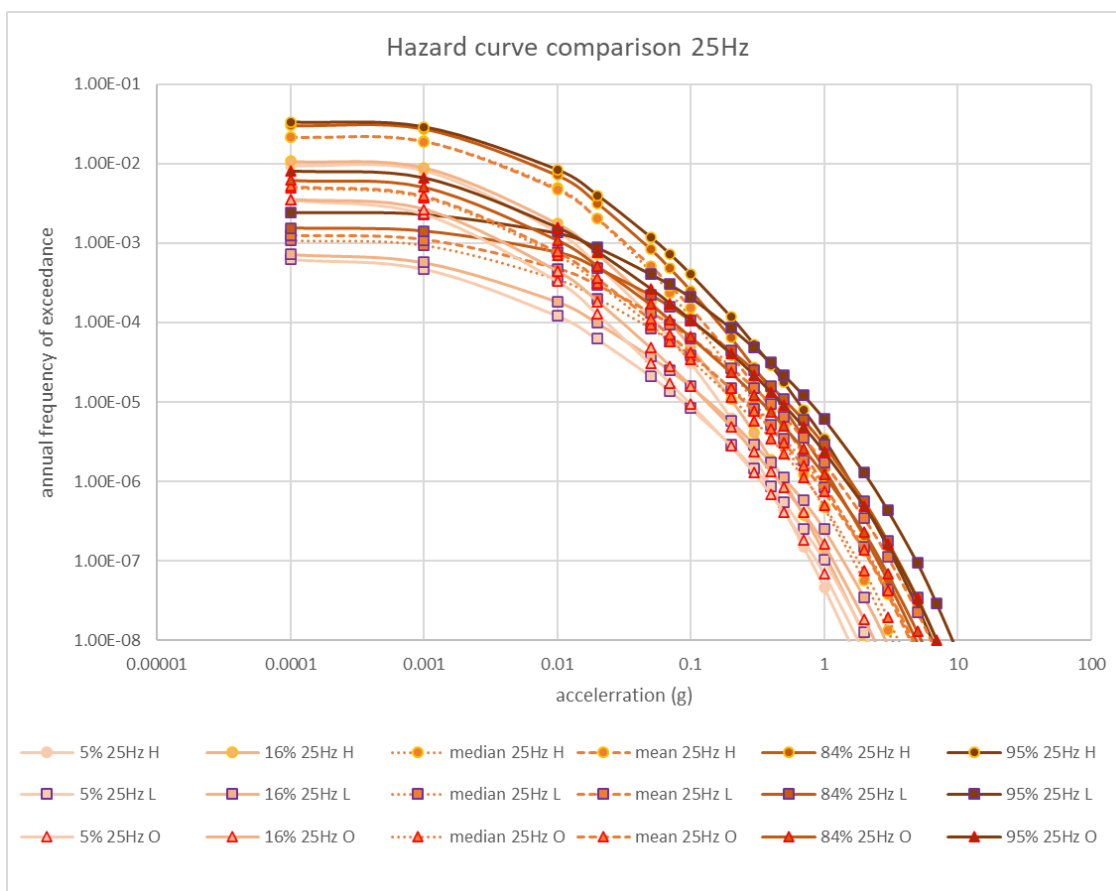
Olkiluoto hazard curves for 5%, 16%, median (50%), mean, 84%, and 95% percentiles for 1Hz, 5Hz, 25Hz, and PGA.



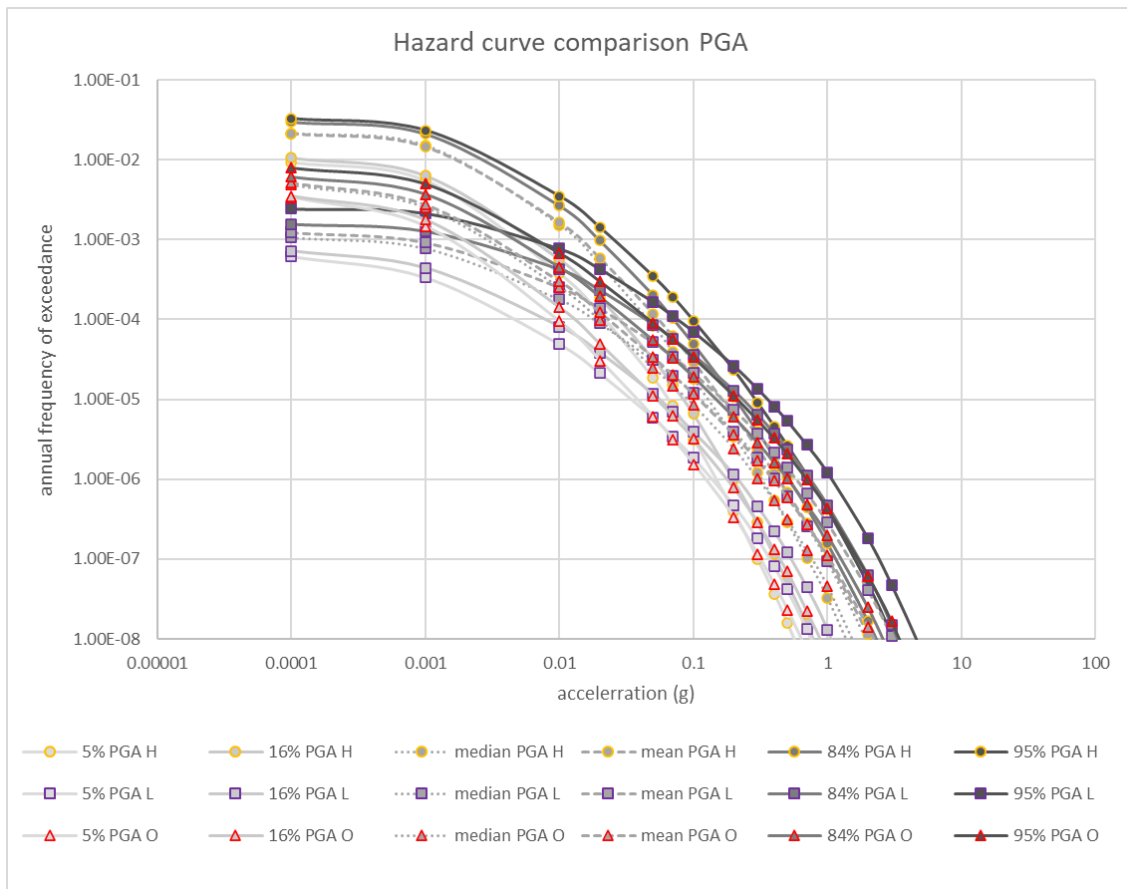
Hazard curve comparison for 5%, 16%, median (50%), mean, 84%, and 95% percentiles for 1Hz for Hanhikivi (H, yellow circle), Loviisa (L, purple square), and Olkiluoto (O, red triangle).



Hazard curve comparison for 5%, 16%, median (50%), mean, 84%, and 95% percentiles for 5Hz for Hanhikivi (H, yellow circle), Loviisa (L, purple square), and Olkiluoto (O, red triangle).



Hazard curve comparison for 5%, 16%, median (50%), mean, 84%, and 95% percentiles for 25Hz for Hanhikivi (H, yellow circle), Loviisa (L, purple square), and Olkiluoto (O, red triangle).



Hazard curve comparison for 5%, 16%, median (50%), mean, 84%, and 95% percentiles for PGA for Hanhikivi (H, yellow circle), Loviisa (L, purple square), and Olkiluoto (O, red triangle).

Certificate Of Completion

Envelope Id: CA5734D3377545AB9F0A0EEBD312EDA5	Status: Completed
Subject: Complete with DocuSign: VTT_R_00978_22	
Source Envelope:	
Document Pages: 42	Signatures: 1
Certificate Pages: 1	Initials: 0
AutoNav: Enabled	Envelope Originator: Erja Schlesier Vuorimiehentie 3, Espoo, .. . P.O Box1000,FI-02044 Erja.Schlesier@vtt.fi IP Address: 130.188.17.16
Envelopeld Stamping: Enabled	
Time Zone: (UTC+02:00) Helsinki, Kyiv, Riga, Sofia, Tallinn, Vilnius	

Record Tracking

Status: Original	Holder: Erja Schlesier	Location: DocuSign
27 January 2023 12:29	Erja.Schlesier@vtt.fi	

Signer Events

Marko Mäkipää
Marko.Makipaa@vtt.fi
Research Team Leader

Teknologian tutkimuskeskus VTT Oy
Security Level: Email, Account Authentication
(None), Authentication

Signature

DocuSigned by:
Marko Mäkipää
EF95EB85E9804AC...

Signature Adoption: Pre-selected Style
Using IP Address: 130.188.17.16

Timestamp

Sent: 27 January 2023 | 12:35
Viewed: 30 January 2023 | 12:04
Signed: 30 January 2023 | 12:08

Authentication Details**SMS Auth:**

Transaction: 66180886120409049197571BA6BA8E30
Result: passed
Vendor ID: TeleSign
Type: SMSAuth
Performed: 30 January 2023 | 12:03
Phone: +358 45 6788723

Electronic Record and Signature Disclosure:

Not Offered via DocuSign

In Person Signer Events**Signature****Timestamp****Editor Delivery Events****Status****Timestamp****Agent Delivery Events****Status****Timestamp****Intermediary Delivery Events****Status****Timestamp****Certified Delivery Events****Status****Timestamp****Carbon Copy Events****Status****Timestamp****Witness Events****Signature****Timestamp****Notary Events****Signature****Timestamp****Envelope Summary Events****Status****Timestamps**

Envelope Sent	Hashed/Encrypted	27 January 2023 12:35
Certified Delivered	Security Checked	30 January 2023 12:04
Signing Complete	Security Checked	30 January 2023 12:08
Completed	Security Checked	30 January 2023 12:08

Payment Events**Status****Timestamps**